



Comparison of Numerical Reduced Order Models of a Generic UCAV Configuration using a New Displacement Grid Method

Baptiste Isnard, Geoffrey Tanguy, Dominique Farcy, Alain Dugeai, Eric Garnier,
Jean-Marc Foucaut

► To cite this version:

Baptiste Isnard, Geoffrey Tanguy, Dominique Farcy, Alain Dugeai, Eric Garnier, et al.. Comparison of Numerical Reduced Order Models of a Generic UCAV Configuration using a New Displacement Grid Method. AIAA AVIATION 2023 Forum, Jun 2023, San Diego, United States. pp.AIAA 2023-3269, <10.2514/6.2023-3269>. <hal-04196249>

HAL Id: hal-04196249

<https://hal.science/hal-04196249v1>

Submitted on 5 Sep 2023

HAL is a multi-disciplinary open access archive for the deposit and dissemination of scientific research documents, whether they are published or not. The documents may come from teaching and research institutions in France or abroad, or from public or private research centers.

L'archive ouverte pluridisciplinaire **HAL**, est destinée au dépôt et à la diffusion de documents scientifiques de niveau recherche, publiés ou non, émanant des établissements d'enseignement et de recherche français ou étrangers, des laboratoires publics ou privés.



HAL Authorization

Comparison of Numerical Reduced Order Models of a Generic UCAV Configuration using a New Displacement Grid Method

Baptiste Isnard ^{*}, Geoffrey Tanguy [†], Dominique Farcy [‡], Alain Dugeai [§], Eric Garnier [¶], Jean-Marc Foucaut ^{||}
Univ. Lille, CNRS, ONERA, Arts et Metiers Institute of Technology, Centrale Lille, UMR 9014 - LMFL - Laboratoire de Mécanique des Fluides de Lille - Kampé de Fériet, F-59000 Lille, France

This paper presents several approaches to model the unsteady and non-linear longitudinal aerodynamics of a UCAV configuration using computational fluid dynamics. The linear and non linear indicial response methods, the linear quasi-steady and the linear unsteady models are part of the aerodynamic reduced order models studied in this work. The methods associated with the identification of the models unknowns are explained and based on URANS simulations with grid displacement. A new method for grid displacement is presented and validated through indicial simulations. This method is twice as fast as the overset method. The generation of databases for the different aerodynamic models is then described. The different reduced order models are then evaluated compared with CFD simulations of pitch forced oscillations for different frequencies and different initial angles of attack. The linear unsteady model appears to be more efficient to model different rotation rates compared with the quasi-steady model. The predictions of the non linear indicial method are the most accurate. The trends and the shapes of the evolution of the longitudinal coefficient are in good agreement with CFD simulations at low angles of attack, whereas for higher angles of attack, some discrepancies are observed especially on the pitch coefficient. The study of implementation costs also shows that the cost of the indicial method is relatively low in view of its accuracy compared with other models.

I. Nomenclature

$a_{i\alpha}$	= regressor affecting the output of the transfert function [-]
b	= half span [m]
B_a, B_p, B_T	= orthonormal basis of the different trihedron [-]
C_A, C_S, C_N	= axial, side and normal force coefficient in body axis [-]
C_D, C_{ya}, C_L	= drag, side and lift force coefficient [-]
C_l, C_m, C_n	= roll, pitch and yaw moment coefficient [-]
C_{i_0}	= static coefficient for parameter i=D, ya, L, l, m, n [-]
$C_{i_\alpha}, C_{i_\beta}$	= static derivative for parameter i=D, ya, L, l, m, n [1/rad]
$C_{i_{p^*}}, C_{i_{q^*}}, C_{i_{r^*}}$	= damping coefficient for parameter i=D, ya, L, l, m, n [1/rad]
$C_{i_{\alpha^*}}, C_{i_{\beta^*}}$	= unsteady dynamic coefficient for parameter i=D, ya, L, l, m, n [1/rad]
$C_{i_\alpha}^{dyn}$	= dynamic coefficient for parameter i=D, ya, L, l, m, n [-]
c_{ref}	= reference chord [m]
f	= frequency [Hz]
$F_{x_a}, F_{y_a}, F_{z_a}$	= drag, side and lift force [N]
$F_{x_p}, F_{y_p}, F_{z_p}$	= axial, side and normal force in body axis [N]
$I_{i_\alpha}, I_{i_{q^*}}$	= Angle of attack and pitch rate indicial responses for parameter i=D, ya, L, l, m, n [1/rad]
M	= Mach number [-]
$M_{x_p}, M_{y_p}, M_{z_p}$	= roll, pitch and yaw moment in body axis [N.m]

^{*}Phd Student, ONERA-DAAA/ELV, baptiste.isnard@onera.fr

[†]Head of Experiment and Flight Limit Unit, ONERA-DAAA/ELV, geoffrey.tanguy@onera.fr

[‡]Engineer, ONERA-DAAA/ELV, dominique.farcy@onera.fr

[§]Engineer, ONERA-DAAA/MSAE, alain.dugeai@onera.fr

[¶]Research director and Deputy director Aerodynamics, Aeroelasticity, Acoustics Department, ONERA-DAAA, eric.garnier@onera.fr

^{||}Research director and Professor in Fluid Mechanics, Centrale Lille, jean-marc.foucaut@centralelille.fr

O	=	center of trihedron [-]
p, q, r	=	roll, pitch and yaw rates [rad/s]
$p^*, \dot{\alpha}^*, f^*, etc.$	=	normalized quantities [-]
P	=	upstream pressure [Pa]
R_a, R_p, R_T	=	aerodynamic, aircraft and terrestrial trihedron [-]
Re	=	Reynolds number [-]
t	=	time [s]
T	=	temperature [K]
s	=	Laplace variable [1/s]
S_{ref}	=	reference surface [m^2]
V	=	freestream velocity [m/s]
x_a, y_a, z_a	=	vectors of the aerodynamic trihedron [-]
x_p, y_p, z_p	=	vectors of the aircraft trihedron [-]
x_T, y_T, z_T	=	vectors of the terrestrial trihedron [-]
α	=	angle of attack (AOA) [rad]
α_k	=	motion amplitude [rad]
β	=	angle of sideslip (AOS) [rad]
Φ, Θ, Ψ	=	roll, pitch and yaw angles [rad]
ρ	=	air density [kg/m^3]
$\tau_{i\alpha}$	=	time constant affecting the output of the transfert function [s]
μ	=	viscosity [Pa.s]
μ_t	=	turbulent viscosity [Pa.s]
ω	=	angular rate [rad/s]

II. Introduction

THE study of an aircraft behaviour in the near-stall or post-stall flight domain allows the quantification of its manoeuvrability and its aerodynamic performances. For manoeuvres in these flight domains, combat aircraft have to be highly manoeuvrable and efficient especially at low speeds and high angles of attack (AOAs). In these conditions, the behaviour of these aircraft is characterised by complex aerodynamics of a vortical nature, including non-linearities and hysteresis phenomena, all coupled with all degrees of freedom of the aircraft [1]. Thus, the unsteady nature of the vortical flow can induce some alterations in the position of local efforts around the aircraft and lead to variations in the overall efforts [2, 3]. Hence, significant changes can be observed in flight stability and manoeuvrability. In order to predict and consider all flight scenarios, it is therefore essential to have an aeromechanical model of the aircraft. The development of a reliable representation of the aerodynamic torsor appears to be the main challenge. Its characterisation is imperative to evaluate the manoeuvrability capabilities of an aircraft and to design effective control laws, allowing to ensure the safety in flight.

Airliner and military aircraft geometries have been extensively studied [4–9] in order to investigate control problems in extended flight domains, particularly at low speeds and high AOAs. In the context of these researches, the study of UCAV (Unmanned Combat Air Vehicle) formulas was at the heart of the collaborative work carried out by NATO from 2010 to 2017. It is during the NATO RTO Task group AVT-161, that the generic UCAV SACCON (Stability And Control Configuration) has been the subject of numerous numerical and experimental works [5–12]. The experience acquired during these various collaborations on the SACCON geometry has enabled to highlight that the traditional, mainly linear, approaches to modelling the aerodynamic torsor are insufficient. Indeed, the non-linear behaviour observed at low speed and high AOA is not modelled [10]. These modelling problems are generally not significant for commercial aircraft manoeuvring at relatively low rotation rates and amplitudes. However, for modern combat aircraft, such as the SACCON geometry, predictions of static and dynamic behaviour fail due to highly non-linear aerodynamic characteristics dominated by vortical flow [13]. This can lead to costly non-linear aerodynamic problems that were not discovered until flight testing [13]. It is now widely recognised that it is essential to improve the modelling of unsteady and non-linear aerodynamic responses during these manoeuvres, both to maximise combat capability and to prevent accidental deviations from controlled flight. To this end, a wide range of linear and non-linear aerodynamic modelling techniques, known as reduced order models (ROMs), have been developed in recent years. Moreover, the emergence of CFD has enriched our understanding on these non-linear unsteady phenomena and has helped to limit the cost of wind tunnel tests and flight testing.

Among the popular ROMs, the linear quasi-steady model [8–10, 14–16] is the most common. The coefficients of

the model are determined by the analysis of forced oscillations at only one given frequency. For a forced oscillation with a different frequency, the rotation rates and the hysteresis phenomena are changed. This leads to a dependence of the model coefficients on the frequency [10, 17]. Therefore, the linear quasi-steady model does not take into account unsteady aerodynamic effects and it is not well suited for the analysis of a high performance aircraft with highly nonlinear and unsteady aerodynamics [13, 18]. This model can be improved in an linear unsteady model by adding a dynamic coefficient, solution of a differential equation, allowing to get away from this frequency dependence [4, 17]. A non-linear model [10] can also be constructed. It is able to model, close to perfection, the evolution of the aerodynamics coefficients at high AOA. However, the model stays dependent on the frequency of the parameters identification. Other models so-called state-space model such as the Goman and Khrabrov model [19] and its derivatives [3, 20], take into account the dependence of the aerodynamic coefficients with physical parameters such as the position of the vortex breakdown but cannot model complex unsteady and non-linear variations. More recently, ROMs based on the physical responses of the dynamic system to a variation in flight parameters have emerged such as the indicial method [5, 14, 21]. Ghoreyshi et al. [22] have brought to light the application of this method based on a CFD grid displacement approach allowing imposed motions which are not achievable in wind tunnel. This model does not depend on the frequency. A linear and non-linear development of the indicial method [5, 14] were applied for the prediction of unsteady aerodynamic loads for imposed trajectories. Comparisons between the indicial method and CFD computations proved its high efficiency. Finally, the last kind of model is based on neural networks (RBF, SRBF) [5, 23]. These models require special training manoeuvres to capture the dynamics of the system of interest. These methods are generally more expensive to develop compared to other approaches and the physical interpretation that follows is much more complex or impossible. So, no matter what ROM is used, its purpose is to quickly calculate the aerodynamic forces and moments of a flight manoeuvre.

The aim of this paper is to determine the performance of different ROMs in terms of accuracy on the predicted aerodynamic coefficients compared with those given by CFD simulations. The computational cost for the implementation of ROMs will also be compared. The present work will focus on the implementation of different ROMs based on numerical simulations only. It will be centered on the study of linear ROMs and indicial method for the modelling of longitudinal coefficients only. This will allow the comparison of classical linear model with the indicial method, which can be considered as one of the most powerful numerical method in the accuracy of the results [5]. In order to reduce the computational cost of the different ROMs, this work presents a new CFD method of grid displacement calculation which does not need any background mesh. This approach proves to be much more efficient than the classical overset method.

The first part of this article presents the different models of the aerodynamic torsor. It describes first the indicial model and then present the differences between linear quasi-steady and unsteady models. The numerical results presented here are mainly focused on longitudinal components. The second part deals with the numerical methods used for the numerical simulations and the identification of the model parameters. The description of the new grid displacement method is detailed and compared with the classical overset method. The third part is devoted to the numerical simulations. First, RANS simulations on the SACCON geometry are compared to wind tunnel results. Then, as validation purpose, a comparison is made between the new displacement method and the overset method based on the simulation of indicial responses. Finally, the indicial responses, the numerical forced oscillations and the coefficients of the different models are estimated. Then, the accuracy and the implementation cost of the ROMs are evaluated by comparison with a CFD calculation.

III. Unsteady Aerodynamics Prediction Models

A. Coordinate System

In flight dynamics, the study of the motion of an aircraft is usually carried out in the Earth's reference frame, which is assumed to be Galilean. However, when the aircraft is moving in airspace, the aerodynamic forces and moments it undergoes can be expressed in different reference frames in order to simplify the solution of the flight dynamics equations. Three trihedrons (Fig. 1) are mainly used: the terrestrial trihedron related to the aircraft $\mathbf{R}_T = (\mathbf{O}, \mathbf{B}_T = (\mathbf{x}_T, \mathbf{y}_T, \mathbf{z}_T))$, the aircraft trihedron $\mathbf{R}_p = (\mathbf{O}, \mathbf{B}_p = (\mathbf{x}_p, \mathbf{y}_p, \mathbf{z}_p))$ and the aerodynamic trihedron $\mathbf{R}_a = (\mathbf{O}, \mathbf{B}_a = (\mathbf{x}_a, \mathbf{y}_a, \mathbf{z}_a))$. The origin of the three trihedrons is chosen arbitrarily on the longitudinal axis of the aircraft. These different trihedrons are linked to each other by the characteristic angles of the flight dynamics. Indeed, the transition from the aircraft trihedron to the aerodynamic trihedron is made by rotations of angle α and β corresponding respectively to the AOA and the angle of sideslip (AOS) of the aircraft (Fig. 1a). Similarly, the transition from the terrestrial trihedron to the aircraft frame is carried out using the Euler angles according to the Tait-Bryan convention, which are the roll angle Φ , pitch angle Θ and yaw angle Ψ (Fig. 1b).

of previous states on the system at any subsequent time. Mathematical models are detailed by Tobak & al. [24, 25] and Reiselthel & al. [26, 27] with the use of the Duhamel superposition. In order to model the aerodynamic response from longitudinal motions, the indicial method takes into account the contributions due to the previous states of AOA and pitch rate which leads to the following expression of the longitudinal coefficients:

$$C_i(t) = C_{i0}(t=0) + \frac{d}{dt} \int_0^t I_{i_\alpha}(t-\tau) \Delta\alpha(\tau) d\tau + \frac{d}{dt} \int_0^t I_{i_{q^*}}(t-\tau) q^*(\tau) d\tau \quad i = L, D, m \quad (3)$$

where C_{i0} denotes the value of the static aerodynamic coefficients in the initial position of the aircraft. $\Delta\alpha(\tau) = \alpha(\tau) - \alpha(t=0)$ is the difference between the AOA at time $t = \tau$ and the AOA at the initial position of the aircraft. The longitudinal indicial responses obtained by a unit step change in the AOA and the normalized pitch rate $q^* = qc_{ref}/V$ are noted respectively I_{i_α} and $I_{i_{q^*}}$, where $i = D, L, m$. The model given by the above equation can be applied to flows that respond linearly to changes in the forcing functions. Linear flight regimes are characterized by a linear variation of the coefficients up to a certain angle after which the flow responds in a non-linear manner due to separated flow or vortical flow effects. Therefore, this equation solves for any time-varying motion within the linear flight regime. However, when considering high performance aircraft such as fighter aircrafts, the manoeuvres of interest are often characterised by variable velocity at AOA potentially extending into the near stall regions. Previous research by the NATO AVT-161 working group has shown that it is important to take into account the variability of the step response with increasing AOA and Mach number [5, 23]. These studies illustrate the inability of the calculated indicial response at low AOA to accurately represent the system dynamics at high angles of attack. So, for non linear flows, the indicial response theory can be extended to a non-linear model using parameterised indicial responses to predict unsteady aerodynamic responses to longitudinal motions [25].

$$C_i(t) = C_{i0}(t=0) + \frac{d}{dt} \int_0^t I_{i_\alpha}(t-\tau, \alpha(\tau)) \Delta\alpha(\tau) d\tau + \frac{d}{dt} \int_0^t I_{i_{q^*}}(t-\tau, \alpha(\tau)) q^*(\tau) d\tau \quad i = L, D, m \quad (4)$$

As shown in the previous equation, the non-linearity of the model is captured by computing the indicial response at different initial AOA. In general, in the case of longitudinal aerodynamics, the AOA indicial response is assumed to vary with the AOA and the Mach number whereas the pitch rate indicial response is assumed to vary only with the Mach number for moderate AOA. However, the accuracy of the model could be improved by including in the database the coupling between the rotation rate and the AOA [14, 28]. Besides, indicial responses obtained from a negative unit step variation could be beneficial to improve the model [14]. The present work focuses on the parameterisation of the two longitudinal indicial responses, I_{i_α} and $I_{i_{q^*}}$, with the AOA only as shown in the previous equation. The non-linear model can be also extended to the lateral coefficients [5]. The validity of this model has been assessed on numerous occasions [5, 14, 23, 29] and has been shown to be in very good agreement with CFD simulations for forced oscillations or imposed trajectories 6-DOF.

2. Linear Quasi-steady Modeling

The most common way of modelling the aerodynamic torsor is to express each coefficient as the sum of sub-coefficients depending on a subset of variables. These sub-coefficients are generally obtained from the first order Taylor series expansion of the aerodynamic forces and moments [8–10, 14–16]. The coefficients are written for $i=(D, \text{ya}, L, l, m, n)$ as:

$$\begin{aligned} C_i &= C_{i0} + \frac{\partial C_i}{\partial \alpha} \Delta\alpha + \frac{\partial C_i}{\partial \beta} \Delta\beta + \frac{\partial C_i}{\partial p^*} p^* + \frac{\partial C_i}{\partial q^*} q^* + \frac{\partial C_i}{\partial r^*} r^* + \frac{\partial C_i}{\partial \dot{\alpha}^*} \dot{\alpha}^* + \frac{\partial C_i}{\partial \dot{\beta}^*} \dot{\beta}^* + \frac{\partial C_i}{\partial \dot{p}^*} \dot{p}^* + \frac{\partial C_i}{\partial \dot{q}^*} \dot{q}^* + \frac{\partial C_i}{\partial \dot{r}^*} \dot{r}^* \\ &= \underbrace{C_{i0}}_{\text{Stat}} + \underbrace{C_{i_\alpha} \Delta\alpha + C_{i_\beta} \Delta\beta}_{\text{Static Derivatives}} + \underbrace{C_{i_{p^*}} p^* + C_{i_{q^*}} q^* + C_{i_{r^*}} r^*}_{\text{Damping Coefficients}} + \underbrace{C_{i_{\dot{\alpha}^*}} \dot{\alpha}^* + C_{i_{\dot{\beta}^*}} \dot{\beta}^*}_{\text{Unsteady Dynamic Coefficients}} + \underbrace{C_{i_{\dot{p}^*}} \dot{p}^* + C_{i_{\dot{q}^*}} \dot{q}^* + C_{i_{\dot{r}^*}} \dot{r}^*}_{\text{Unsteady Dynamic Damping Coefficients}} \end{aligned} \quad (5)$$

Where $C_{i0} = C_{i0}(\alpha_0, \beta_0)$ represents the initial static aerodynamic coefficient and $\Delta\alpha = \alpha(t) - \alpha_0$ with $\alpha_0 = \alpha(t=0)$. Similarly, $\Delta\beta = \beta(t) - \beta_0$. In general, it is considered that the sub-coefficients vary according to the incidence α , the sideslip β and/or the Mach number M , in other words $C_{ik} = C_{ik}(\alpha, \beta, M)$ for $k = (\alpha, \beta, p^*, q^*, r^*, \dot{\alpha}^*, \dot{\beta}^*, \text{etc.})$. In the present work, $C_{ik} = C_{ik}(\alpha)$ depends only with the AOA. The above equation is expressed in terms of the following normalized quantities:

$$p^* = \frac{p(t)b}{V} \quad q^* = \frac{q(t)c_{ref}}{V} \quad r^* = \frac{r(t)b}{V} \quad \dot{\alpha}^* = \frac{\dot{\alpha}c_{ref}}{V} \quad \dot{\beta}^* = \frac{\dot{\beta}b}{V} \quad \dot{p}^* = \frac{\dot{p}b^2}{V^2} \quad \dot{q}^* = \frac{\dot{p}c_{ref}^2}{V^2} \quad \dot{r}^* = \frac{\dot{r}b^2}{V^2}$$

The impact of the deflection of control surfaces is not studied in this work. The literature often presents a decoupling between longitudinal coefficients and lateral quantities (β , p , r). Indeed, under the assumption that the influence of the AOS and the lateral components of the angular velocity (p and r) of the longitudinal coefficients are negligible, it is possible to write:

$$C_i = C_{i_0} + C_{i_\alpha} \Delta\alpha + C_{i_{q^*}} q^* + C_{i_{\dot{\alpha}^*}} \dot{\alpha}^* + C_{i_{\dot{q}^*}} \dot{q}^* \quad i = L, D, m \quad (6)$$

This kind of representation is widely used in the aeronautical industry for its simplicity of use and identification. However, the linear quasi-steady model is only efficient in the linear flight domain corresponding to low AOA flight. It does not allow the representation of non-linearities and induced couplings, which limits its use when flow separations or vortex breakdown occurs. This model can be extended to lateral coefficients by assuming that the influence of the pitching angular velocity q is negligible.

3. Linear Unsteady Modeling

As seen above, the linear quasi-static model does not take into account the dependence of the aerodynamic derivatives on unsteady aerodynamic effects. However, a variant of this method consists in adding a dynamic component to the coefficients in order to model these unsteady effects [4, 17]. The expression of the unsteady longitudinal coefficients are presented below:

$$C_i = C_{i_0} + C_{i_\alpha} \Delta\alpha + C_{i_{q^*}} q^* + C_{i_{\dot{\alpha}^*}} \dot{\alpha}^* + C_{i_{\dot{q}^*}} \dot{q}^* + C_{i_\alpha}^{dyn} \quad i = L, D, m \quad (7)$$

It consists of classical aerodynamic quasi-steady derivatives to which are added dynamic terms for the most significant coefficients. These dynamic coefficients are solutions of a first order differential equation depending on the variation of the AOA [17]:

$$\dot{C}_{i_\alpha}^{dyn} + \frac{1}{\tau_{i_\alpha}} C_{i_\alpha}^{dyn} = a_{i_\alpha} \dot{\alpha} \quad i = L, D, m \quad (8)$$

Where τ_{i_α} and a_{i_α} are AOA-dependent quantities. The fact that the constant depends on the derivative of the incidence allows to take into account the temporal dissymmetries of the detachment / reattachment of the flow on the upper surface [4]. In Laplace space, the dynamic coefficients are represented by the following transfer functions:

$$C_{i_\alpha}^{dyn}(s) = \frac{a_{i_\alpha} s}{1 + \tau_{i_\alpha} s} \alpha(s) \quad i = L, D, m \quad (9)$$

Where s represents the Laplace parameter. Adding this dynamical coefficient is equivalent to take into account the previous transfert function which capture all the frequency effects and provides frequency independent coefficients and parameters. The coefficients of this model are identified using forced oscillations at different frequency [4].

IV. Geometry and Description of Numerical Methods

A. SACCON Geometry

The geometry of the generic UCAV named SACCON (Stability And Control CONFIGuration) was developed specifically for the RTO/AVT-161 research group. It was designed with a 53° sweep angle. The numerical study carried out here is based on the dimensions of the model designed by ONERA in 2010. This geometry is simply reduced by 35% compared to those used by DLR and NASA. The overall shape of the SACCON and its dimensions are presented in figures 2a and 2b. The ONERA model of the SACCON has a reference chord $c_{ref} = 0.3113m$ and a half span $b = 0.5m$. The reference surface is $S_{ref} = 0.3253m^2$. Finally, the calculated moments are expressed at the moment rotation point (MRP) chosen at $x/l = 56.56\%$ corresponding to a point distant from the nose of the aircraft of 0.390m. This study is focused on the SACCON round leading edge (RLE) configuration for which the leading edge is evolving.

B. CFD Solver

The flow solver used for this study is the elsA code developed by the ONERA. The elsA code is a CFD code, based on a cell-centered "finite volume" approach, dedicated to the numerical simulation of internal and external flows for compressible and viscous fluids on two- and three-dimensional meshes. In particular, it allows parallel calculations on several processors for meshes with complex geometries in structured, unstructured or hybrid form. More details on the capabilities of this solver are described in Cambier & al. [30, 31]. In order to accelerate the solution of the discretised system, the elsA code uses an implicit method allowing a high Courant-Friedrichs-Lewy number (>1). The diversity of

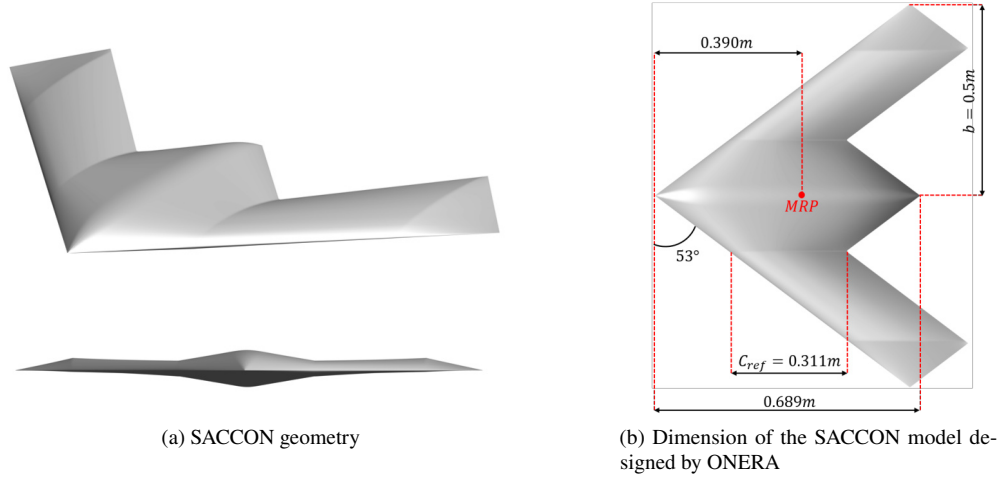


Fig. 2 Geometry of the SACCON (ONERA model)

models and simulation techniques present in this CFD code allows to adapt the simulations according to the problems and the different physical mechanisms encountered. In the context of our study, RANS and URANS calculations are performed. The numerical parameters used for these simulations are detailed later.

C. Computational Grid and Numerical Parameters

For this study, RANS and URANS simulations were performed in a cylindrical domain of radius 20m and height 40m with the SACCON geometry in its center. The objective was to have more than 20 times the size of the SACCON between the geometry and the edge of the domain in all directions to minimise the risk of reflection. The center of gravity of the SACCON is chosen as the origin of the frame. The mesh generated for this study is a multi-block structured mesh (Fig. 3). The topology of the mesh is C-H in order to take into account the thickness of the trailing edge of the UCAV. The mesh presented in this paper is the result of a mesh convergence study (Richardson's method [32]) in order to obtain results in agreement with the experimental results for a reasonable or acceptable restitution time. Particular attention has been paid to the resolution of the leading edge, the trailing edge and the boundary layer in order to correctly capture the origin of the vortices (Fig. 3a). The height of the first cell is constant around the UCAV at 0.003 mm to obtain a y^+

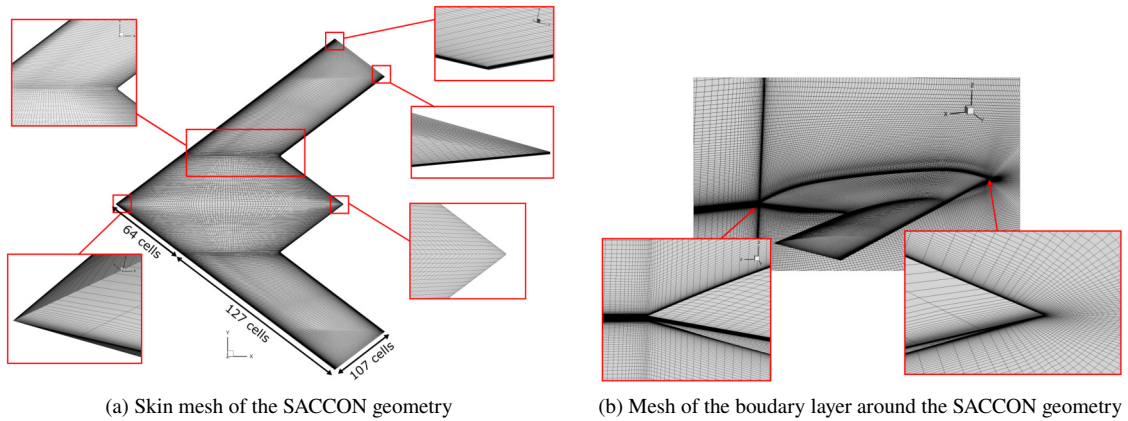


Fig. 3 Mesh around the SACCON geometry

close to 1. To allow a correct resolution of the viscous sub-layer and thus to correctly simulate the boundary layer and the vortex systems, the boundary layer is composed of 70 meshes by 25mm (expansion ratio 1.1) (Fig. 3b). The total mesh size is about 25.5 million cells. In order to better calibrate our simulations, a sensitivity study of the aerodynamic

coefficients on the numerical parameters has been performed. Among the different turbulence models and discretization schemes tested, the use of the Spalart-Allmaras turbulence model [33] with the Jameson scheme ($k_2=0$, $k_4=0.016$ to minimize the damping effects) [34] proved to be the most efficient. The elsA solver solves the turbulence equations in a decentered way. So, the Harten parameter is set to a small value (0.01) to obtain good accuracy. An additional Martinelli correction (0.3) has also been added to improve the performance of the model and avoid oscillation of the residuals. All calculations are performed in fully turbulent mode. Finally, the use of a low-Mach preconditioning [35, 36] is not used for this study due to degradation of the results. Flow boundary conditions are used at the inlet, outlet and radial boundary of the domain with infinite flow values corresponding to those in Table 1. The SACCON surface is considered as an adiabatic rigid wall. For the RANS simulations, the equations are solved using a backward Euler scheme and a CFL of 25 is applied to ensure a satisfactory speed of convergence. The results of these static simulations are obtained after 90,000 iterations in the present work. URANS calculations for indicial responses or forced oscillations started from the steady-state solution of RANS simulation. RANS and URANS computations are launched on 224 cores.

Parameters	Values	Parameters	Values
Mach number M	0.15	Reynolds R_e	$1.09 \cdot 10^6$
AOA α	$0-28^\circ$	AOS β	$0-15^\circ$
Upstream Pressure P	101325 Pa	Density ρ	1.2252 kg/m^3
Temperature T	288 K	Viscosity μ	$1.7345 \cdot 10^{-5} \text{ Pa.s}$
Upstream Velocity V	51.28 m/s	Turbulent Viscosity μ_t	$2.9877 \cdot 10^{-5} \text{ Pa.s}$

Table 1 SACCON simulation parameters

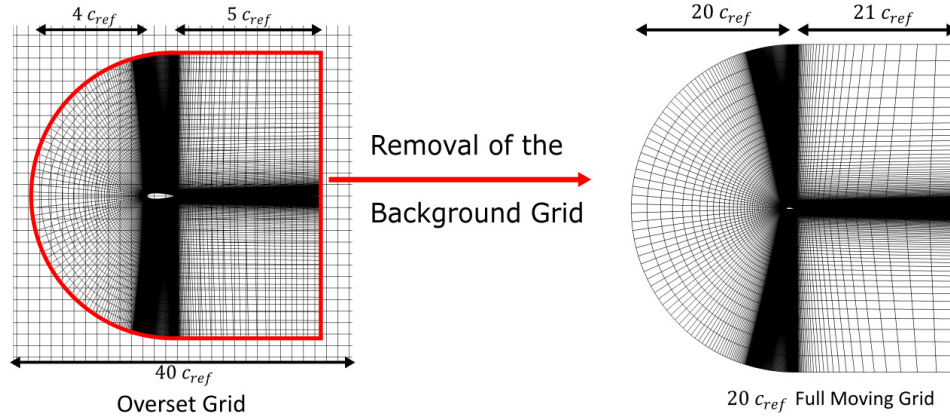


Fig. 4 Example for a NACA0012 profile: overset mesh (left), mesh used for the FMG method (right)

D. Overset Grid Approach

The elsA software allows to solve unsteady flow around a static or spatially moving geometry. Indeed, it is possible to carry out CFD simulations with possibly significant movement such as a complete flight manoeuvre or forced oscillations to reproduce wind tunnel tests [5]. Classically, this kind of simulation is performed using an overset grid method. This technique is based on the superposition of several meshes generated individually, thus forming a composite domain [37–39]. In practice, a relatively coarse cartesian mesh forms the background of the domain and does not take into account the geometry of the object of study. A second mesh, finer and body-fitted to the geometry of the object, called chimera, is then superimposed on top of the background mesh using a grid assembly process (Fig. 4 left). During a simulation, a transfer of information takes place at each iteration between the background mesh and the chimera mesh. Indeed, at the junction between the meshes, the boundary conditions are interpolated to ensure the continuity of the quantities. The size of the cells between the two meshes, especially in this interpolation zone, must be similar in order to improve the transition of the calculation between them. These interpolation zones (overlapping of around 4 cells here)

are defined during the assembly process in the same way as the masking zones which avoid calculating the solution on the parts of the background mesh that are covered. During a dynamic simulation, the chimera mesh must be able to move inside the background mesh, at each time step, without any mesh deformation, in a free or specified way over its six degrees of freedom (6DoF). In the case of an imposed motion, the trajectory is specified from an input file. The latter contains the location, at each time step, of the center of gravity of the aircraft. The orientation of the aircraft is also specified using the roll, pitch and yaw angles. Thus, for each iteration, the mesh is updated, by moving the mesh blocks, according to the displacement of the center of gravity and the orientation of the aircraft that are pre-calculated. Moreover, the interpolation and masking zones are uploaded too. In the case of our simulations, a flow velocity is imposed on the fluid $\mathbf{V}_\infty = -V_\infty \mathbf{x}_T$ in order to reduce the displacement of the mesh in the domain. Indeed, by noting $\mathbf{V}_{\text{rel}} = V_\infty \mathbf{x}_T$ the real velocity of the center of gravity of the plane in the aerodynamic frame, the instantaneous location of the plane is then defined from the absolute velocity vector $\mathbf{V}_{\text{rel}} + \mathbf{V}_\infty$. This method is then very well adapted to treat both forced oscillation movements and indicial responses.

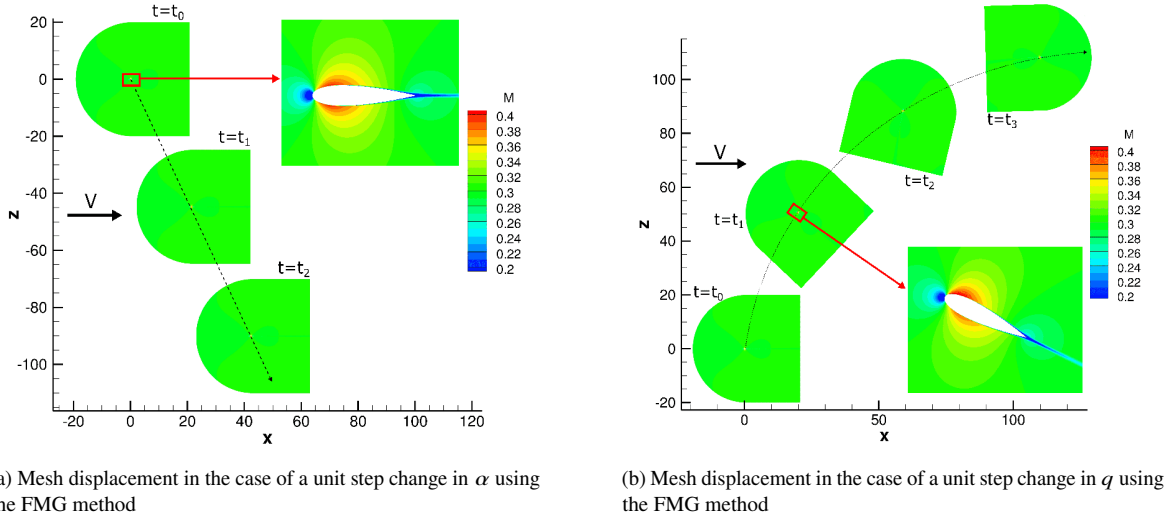


Fig. 5 Schematic representation of the mesh displacement for the identification of indicial responses using the FMG method

E. Full Moving Grid Approach

Although well known and efficient, the overset grid method has the drawback of being expensive in terms of calculation time. This is mainly due to determination of masking zone and the fields interpolations between the meshes. Specific methods such as the ALE (Arbitrary Lagrangian-Eulerian) methods make it possible to avoid using the overset method for certain movements. The ALE method allows to simulate efficiently forced oscillations or ramps, without moving the mesh, by selecting a rotation point around which the boundary conditions on the edges of the domain are modified at each time step. However, for the simulation of more complex motion such as complete flight manoeuvre or identification of indicial response, this method is not adapted. A new method has been developed to limit the waste of time and free ourselves from the interpolation constraints of the overset method, while being able to realize any kind of trajectory. For this purpose, the new method presented here named Full Moving Grid (FMG) does not require any background mesh. Thus, only the fine mesh adjusted to the study object is kept (Fig. 4 right). As a result, the entire mesh domain is mobile and can reproduce the same trajectory as in the overset method. Thus, movements are no longer restricted by the size limitation of the background mesh, and no more interpolation and masking between various superimposed meshes is required. However, at each time step, the previous flow field solution is interpolated in the new mesh position. To this end, a no-reflection condition supplied by the imposed flow, independently of the block motion, is applied to the boundary of the domain. The solver elsA updates the boundary conditions automatically by aligning the incoming flow with the initially chosen incoming velocity vector. For the FMG method, the displacement and orientation of the mesh over the time works on the same principle as the overset method. An example of mesh

displacement simulation with FMG is shown in figure 5. Indeed, figure 5a and figure 5b represent respectively in a schematic way the mesh displacement obtained to determine the indicial response following a unit step variation in α and q as stipulated by the method developed by Ghoreyshi et al. [23, 40]. The validity of this new method is studied in the following section in order to compare its results and its computational time cost with the overset method. The objective is to show that the FMG method can achieve identical movements to the overset method while reducing the computation time of 6DOF manoeuvre simulations.

F. Determination of a trajectory with imposed conditions

In order to obtain an imposed trajectory, the temporal evolution of the following flight quantities have to be prescribed $D = (V_{rel}, p, q, r, \alpha, \beta)(t)$. The aeromechanical behaviour of the aircraft in flight is characterised by the position of its centre of gravity as well as by its orientation. For CFD simulations, the flight dynamics equations are written in the relative speed frame $\mathbf{V}_{rel} + \mathbf{V}_\infty$ where the velocity of the upstream flow V_∞ is supposed constant. Hence, to obtain the imposed trajectory, it is necessary to determine the evolution of the unknown $W = (x_G, y_G, z_G, \Psi, \Theta, \Phi)$ by solving the following differential equations:

$$\begin{aligned} \dot{x}_G &= -V_\infty + V_{rel}(C_\alpha C_\beta C_\Psi C_\Theta + S_\beta(C_\Psi S_\Theta S_\Phi - S_\Psi C_\Phi) + C_\beta S_\alpha(C_\Psi S_\Theta C_\Phi + S_\Psi S_\Phi)) \\ \dot{y}_G &= V_{rel}(C_\alpha C_\beta S_\Psi C_\Theta + S_\beta(S_\Psi S_\Theta S_\Phi + C_\Psi C_\Phi) - C_\beta S_\alpha(S_\Psi S_\Theta C_\Phi - C_\Psi S_\Phi)) \\ \dot{z}_G &= -V_{rel}(C_\alpha C_\beta S_\Theta - S_\beta C_\Theta S_\Phi - C_\beta S_\alpha C_\Theta C_\Phi) \\ \dot{\Psi} &= \frac{1}{C_\Theta}(q S_\Phi + r C_\Phi) \\ \dot{\Theta} &= q C_\Phi - r S_\Phi \\ \dot{\Phi} &= p + \tan\Theta(q S_\Phi + r C_\Phi) \end{aligned} \quad (10)$$

Where $C_\alpha = \cos(\alpha)$ and $S_\alpha = \sin(\alpha)$. This system of equations is equivalent to $\dot{W} = f(W)$. Once the flight parameters have been set, the integration is performed with time-centered implicit integration scheme and gives the position and the orientation of the aircraft at each time step with:

$$W_{n+1} = W_n + \Delta t \left(I_d - \frac{\Delta t}{2} \frac{\partial f}{\partial W} \right)^{-1} f(W_n) \quad (11)$$

where Δt is the time step and I_d is the identity matrix.

G. System Identification Methods

1. For Indicial Responses

Indicial responses are difficult or impossible to obtain in wind tunnel because of experimental constraints and kinematical limitations. For this reason, indicial responses were analytically modeled by exponential functions [21]. However, these analytical expressions are not valid for aircraft configurations that exhibit three-dimensional upper surface vortices. With the emergence of CFD, the responses of the system to a variation have become more accessible. Indeed, Ghoreyshi et al. [40] developed a CFD grid displacement method to impose an aircraft motion and to identify linear and non-linear indicial responses. For this, a motion of the study object is specified from a motion input file defining its position and orientation at each time step. In the case of longitudinal coefficients, only the changes in AOA and pitch rate are useful for the application of the model. Thus, to determine the AOA indicial response I_{i_α} corresponding to a step α_k on the AOA, a movement satisfying the following conditions must be applied:

$$\alpha(t) = \begin{cases} \alpha = \alpha_0 + \alpha_k & \text{if } t > 0 \\ \alpha = \alpha_0 & \text{else} \end{cases} \quad p, q, r = 0 \text{ rad/s}, V_{rel} = V_\infty, \beta = \beta_0 = 0 \text{ rad}$$

The AOA changes brutally over time while the other quantities are kept constant. Solving the equations of motion (Eq. 10) with these constraints gives $\Psi = \Phi = 0$ and $\Theta = \alpha_0$ which leads to no rotation and the translation is given by:

$$\begin{aligned} \dot{x}_G &= V_\infty(C_{\alpha_k} - 1) \\ \dot{y}_G &= 0 \\ \dot{z}_G &= V_\infty S_{\alpha_k} \end{aligned} \quad (12)$$

Thus, the aircraft starts to move from $t = 0s$ to the right and downwards (Fig. 5a). The downwards translation allows the AOA to be increased, and the translation to the right maintain constant the velocity of the flow perceived by the aircraft by the law of velocity composition. Furthermore, no rotation is present. Variations in aerodynamic loads are caused entirely by a variation in AOA. Hence, during this motion, the longitudinal coefficients are written as a function of the AOA expressed thanks to the Heaviside function $H_e(t)$:

$$C_i(t) = C_{i_0} + \frac{d}{dt} (I_{i_\alpha} \wedge \alpha_k H_e) = C_{i_0} + \alpha_k I_{i_\alpha} \wedge \delta(t) = C_{i_0} + \alpha_k I_{i_\alpha}(t, \alpha) \quad (13)$$

Where \wedge denotes the convolution product. The indicial response over time is therefore expressed as:

$$I_{i_\alpha}(t, \alpha) = \frac{C_i(t) - C_{i_0}}{\alpha_k} \quad (14)$$

Similarly, to determine the indicial response $I_{i_{q^*}}$ corresponding to a change in pitch rate q_k , a movement satisfying the following conditions must be applied:

$$q(t) = \begin{cases} q = q_k \text{ rad/s} & \text{if } t > 0 \\ q = 0 \text{ rad/s} & \text{else} \end{cases} \quad p, r = 0 \text{ rad/s}, V_{rel} = V_\infty, \alpha = \alpha_0, \beta = \beta_0 = 0 \text{ rad}$$

This time, this is the rotation rate which changes brutally while the other quantities are kept constant. Solving the equations of motion with these constraints gives $\Psi = \Phi = 0$ and $\Theta = \alpha_0 + q_k t$ which leads to a pitch rate and the translation is given by:

$$\begin{aligned} \dot{x}_G &= V_\infty (C_{tq} - 1) \\ \dot{y}_G &= 0 \\ \dot{z}_G &= V_\infty S_{tq} \end{aligned} \quad (15)$$

Thus, the aircraft moves and rotates simultaneously (Fig. 5b). At $t = 0s$, the aircraft starts to rotate due to the pitch rate variation inducing also an AOA variation. To counteract this increase, the aircraft is also shifted to the right and upwards. Thus, the velocity and angle of attack are kept constant over time. The indicial function is obtained in the same way and is written:

$$I_{i_{q^*}}(t, \alpha) = \frac{C_i(t) - C_{i_0}}{q_k^*} \quad (16)$$

This method therefore allows the influence of each of the parameters (here α and q^*) on the aerodynamic loads to be completely decoupled from other parameters according to the imposed motion. The indicial method is therefore a non-intrusive method, easy to implement, allowing to simulate any arbitrary trajectories at any speed. However, as previously mentioned, the major drawback of this model is that the degree of non-linearity resolved increases with the number of indicial responses identified in the flight domain. To capture these non-linearities, a large number of simulations must be performed. The number of simulations therefore increases strongly with the accuracy of the desired sampling. So, indicial functions must be generated for each combination of AOA (if more precision is required each combination of AOA, AOS and Mach number can be solved). This is therefore very costly in terms of computation time and the cost of implementation can become much higher than the cost of CFD simulation for several manoeuvres. In order to reduce this cost for the creation of the model, Ghoreyshi et al.[41] have used a special approach of modelling based on time-dependent substitutes by Surrogate-based models. Thus, it allows to interpolate, at each time step, the value of the unsampled indicial responses at a new point (α, β, M) from the database of the already computed indicial functions using kriging interpolation models. The kriging interpolations are performed with the MultiFiCoKriging algorithm of the open source library OpenMDAO [42].

2. For Linear Quasi-Steady Model

The identification of the different terms of the longitudinal quasi-steady model is made possible by the study of forced oscillations in pitch. During forced oscillations with amplitude α_k around a mean value of the AOA α_0 at a frequency f , the angle of attack over time is written $\alpha(t) = \alpha_0 + \alpha_k \sin(2\pi f t)$. Moreover, the quantities p and q are 0

values while $\dot{\alpha}(t) = q(t)$. The longitudinal coefficients, namely the drag coefficient C_D , the lift coefficient C_L and the pitching moment coefficient C_m can be written:

$$\begin{aligned} C_i(t) &= C_{i_0} + \left(C_{i_\alpha} - \omega^{*2} C_{i_{q^*}} \right) \Delta\alpha + \left(C_{i_{q^*}} + C_{i_{\dot{\alpha}^*}} \right) q^* \\ &= C_{i_0} + C_{i_{\alpha+q^*}} \Delta\alpha + C_{i_{q^*+\dot{\alpha}^*}} q^* \end{aligned} \quad (17)$$

Where the parameter $\omega^* = \frac{\omega c_{ref}}{V} = \frac{2\pi f c_{ref}}{V}$ corresponds to the normalized frequency for the longitudinal forced oscillations. This formulation highlights the appearance of coupled terms that cannot be determined separately with this kind of oscillation. Thus, the quantity $C_{i_{\alpha+q^*}}$ will be noted as the global static derivative corresponding to the coupling between the static derivative C_{i_α} and the dynamic damping coefficient $C_{i_{q^*}}$. Similarly, the quantity $C_{i_{q^*+\dot{\alpha}^*}}$ is defined as the global damping coefficient corresponding to the coupling between the damping coefficient $C_{i_{q^*}}$ and the dynamic derivative $C_{i_{\dot{\alpha}^*}}$.

$$C_{i_{\alpha+q^*}} = C_{i_\alpha} - \omega^{*2} C_{i_{q^*}} \quad (18)$$

$$C_{i_{q^*+\dot{\alpha}^*}} = C_{i_{q^*}} + C_{i_{\dot{\alpha}^*}} \quad (19)$$

The global static derivative and the global damping coefficients are determined by the method of least squares over 1 cycle-average at one mean value of the AOA centered in α_0 and one frequency f . It does not take into consideration the influence of the frequency on the coefficients.

3. For Linear Unsteady Model

The previous paragraph has shown that from the study of forced oscillations, only coupled coefficients can be determined. The linear unsteady model can also be written in terms of coupled coefficients:

$$C_i(t) = C_{i_0} + C'_{i_{\alpha+q^*}} \Delta\alpha + C'_{i_{q^*+\dot{\alpha}^*}} q^* + C_{i_\alpha}^{dyn} \quad i = L, D, m \quad (20)$$

However, forced oscillation can be studied in the frequency domain. Then, the Laplace coefficient can be written as $s = i\omega$ where ω corresponds to the pulsation of the movement. The dynamical coefficient (Eq. 9) becomes:

$$C_{i_\alpha}^{dyn} = \frac{a_{i_\alpha} \tau_{i_\alpha}^2 \omega^2}{1 + \tau_{i_\alpha}^2 \omega^2} \Delta\alpha + \frac{a_{i_\alpha} \tau_{i_\alpha}}{1 + \tau_{i_\alpha}^2 \omega^2} \frac{V}{c_{ref}} q^* \quad i = L, D, m \quad (21)$$

That's why, in the case of forced oscillations, it is possible to find a formulation similar to the quasi-steady model by replacing the equation (21) in the equation (20):

$$C_i(t) = C_{i_0} + \left(C'_{i_{\alpha+q^*}} + \frac{a_{i_\alpha} \tau_{i_\alpha}^2 \omega^2}{1 + \tau_{i_\alpha}^2 \omega^2} \right) \Delta\alpha + \left(C'_{i_{q^*+\dot{\alpha}^*}} + \frac{a_{i_\alpha} \tau_{i_\alpha}}{1 + \tau_{i_\alpha}^2 \omega^2} \frac{V}{c_{ref}} \right) q^* \quad i = L, D, m \quad (22)$$

And so, its possible to find in the case of forced oscillations, an equivalence between quasi-steady coefficients and those from the linear unsteady model:

$$\begin{aligned} C_{i_{\alpha+q^*}} &= C'_{i_{\alpha+q^*}} + \frac{a_{i_\alpha} \tau_{i_\alpha}^2 \omega^2}{1 + \tau_{i_\alpha}^2 \omega^2} \\ C_{i_{q^*+\dot{\alpha}^*}} &= C'_{i_{q^*+\dot{\alpha}^*}} + \frac{a_{i_\alpha} \tau_{i_\alpha}}{1 + \tau_{i_\alpha}^2 \omega^2} \frac{V}{c_{ref}} \end{aligned} \quad (23)$$

These global coefficients are then independent of the frequency. For the application of the model the parameters $C_{i_{\alpha+q^*}}$, $C'_{i_{q^*+\dot{\alpha}^*}}$, a_{i_α} and τ_{i_α} must be determined. The method of the least squares is then applied on forced oscillations of different frequency centered on the same mean AOA. The huge shortcomming of this model structure is that it requires a large number of trials to end up with a representative model. Moroeover, some modelling difficulties can be expected for modern fighter aircraft configurations that generate many non-linearities [4].

V. Results

A. Static Results

The results of the RANS simulations obtained in the present work are compared with the experimental results obtained by ONERA and DLR (Fig 6). The CFD calculations are particularly close to the experimental results up to moderate AOAs around $16-18^\circ$ and that for different AOSs up to 15° . For higher AOAs, more differences are observed between the experimental and numerical values, but the trends in the evolution of the coefficients are maintained. The largest deviations are obtained for the pitching moment. This slope shifts can be explained by the absence of the sting in the simulations [5]. This absence can also explain the shift in lift coefficient. When the AOS increases, notable evolutions are observable on the trends of the lateral coefficients C_y , C_l and C_n while the impact on the lift and drag coefficients is minimal. However, for the pitch coefficient, the increase of the AOS causes a smoothing of the non-linearity becoming less abrupt between 12° and 18° . This phenomenon can also be observed experimentally. This comparison between simulation and wind tunnel tests shows that CFD allows to obtain correct global forces and moments and correct trends at high AOA in relatively efficient way, without accurately predicting the pitching moment and that whatever the AOS. The choice of numerical parameters and the mesh used in the present work allow to

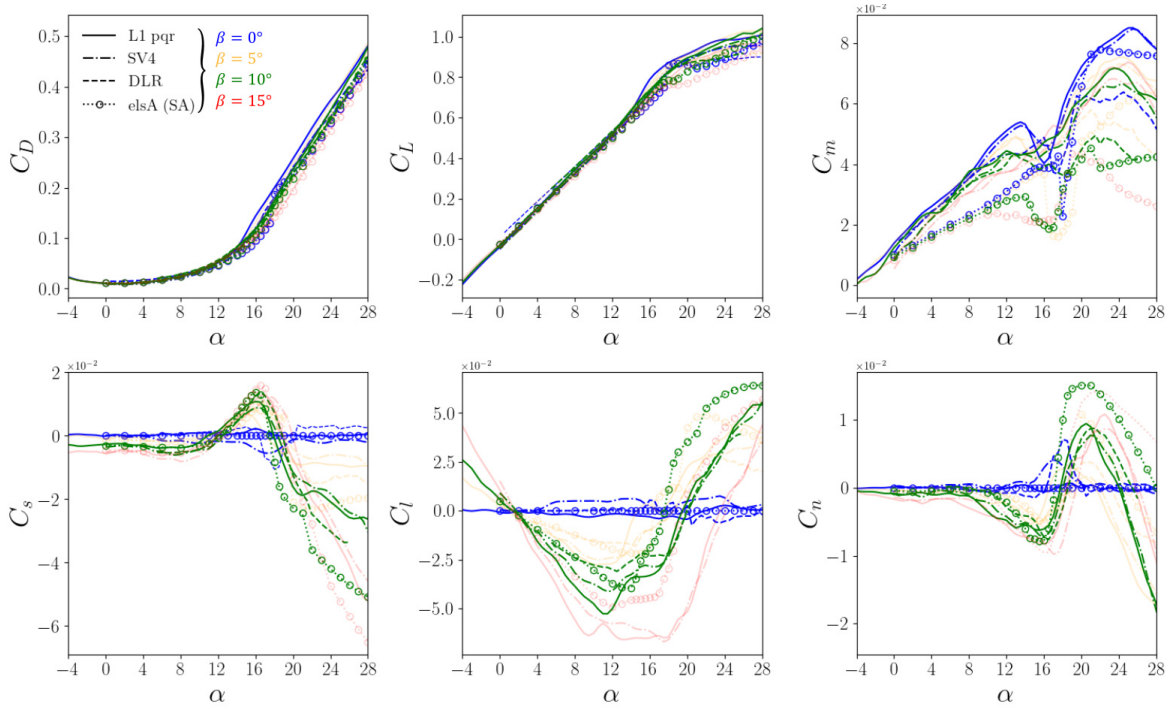


Fig. 6 Comparison between numerical (present work) and experimental static coefficients (ONERA 2011 and DLR TN2373) as a function of AOA for different AOSs at $M = 0.15$ and $Re = 1.09 \cdot 10^6$

observe the formation of the different vortices (Fig. 7) on the upper surface of the SACCON which are also observed experimentally [7]: the apex vortex, the tip vortex and the thickness vortex. The dynamics of these different vortices is caught by CFD simulations, from their formation to their breakdown, via their separation and fusion. Indeed, the apex and tip vortex appear at an AOA of 10° (Fig. 7 top left). Then around 14° , the apex vortex splits in two at the wing kink giving rise to the thickness vortex while the tip vortex intensifies and slowly rises towards the apex (Fig. 7 top middle). By increasing the AOA up to 16° , the different vortices become more intense and the tip vortex continues its ascent towards the apex (Fig. 7 top right). From 18° , the tip vortex rises abruptly towards the apex and merges with the thickness vortex and causes the non-linearities observed in the coefficients (Fig. 7 bottom left). Then, the increase of the AOA leads to the rise to the apex of the tip vortex, its merging with the apex vortex and its gradual vortex breakdown (Fig. 7 bottom right). However, the simulations, compared with experimental data [7]) fail to capture the development of these vortices for the correct angles of attack and their correct positioning on the upper surface. As a result, the local C_p values are not correct, which leads to differences in the pitching moment values and not in the lift and drag forces.

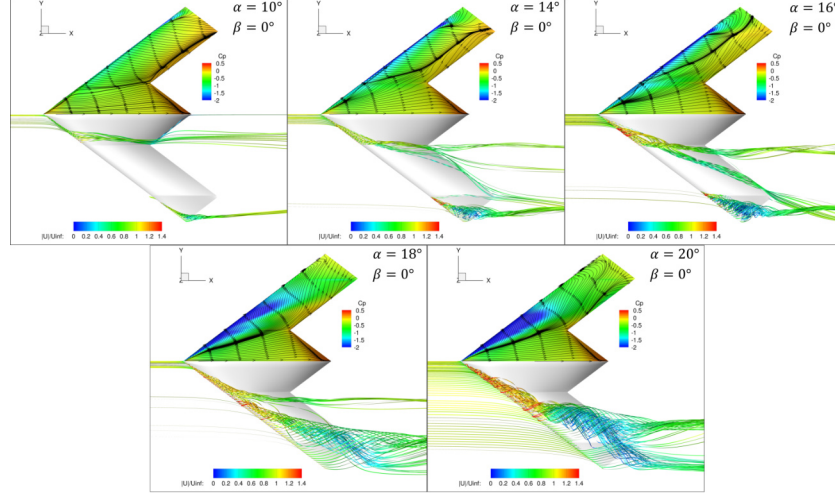


Fig. 7 Visualisation of the vortices on the upper surface of the SACCON obtained numerically for different AOA at $M = 0.15$ and $Re = 1.09 \cdot 10^6$

B. Numerical Validation of the Full Moving Grid Approach

This part aims to compare the overset method with the FMG calculation method for unsteady simulations in order to verify its results and ensure its efficiency. First of all, the comparison of steady-state results obtained with the overset method are identical to those presented in the previous section for the FMG mesh but are not presented in this paper. The computational time for RANS simulation are equivalent for both methods, the FMG method is slightly faster (Table 2). URANS calculations started from the steady-state solution of RANS simulation. The comparison between the overset and FMG method will be made on the SACCON geometry on the basis of indicial simulations (presented in section B.1) for a unit step variation in AOA at zero rotation rate and then for a variation in rotation rate for a fixed AOA (Fig. 8 and 9). The sensitivity of indicial responses to mesh size, time step, time resolution method and number

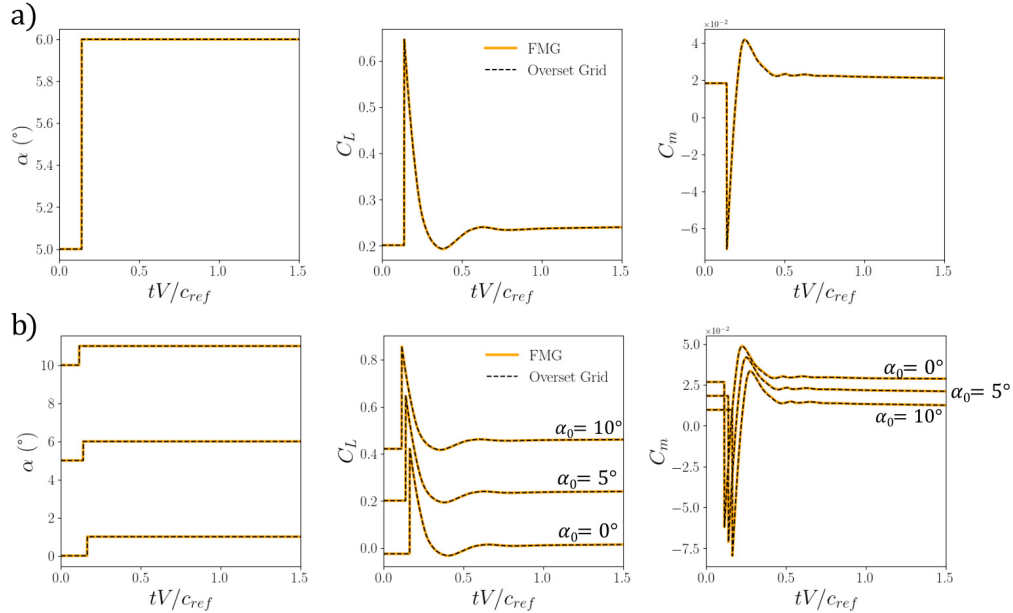


Fig. 8 Comparison of the time evolution of the lift and pitch coefficients due to a unit step change in the AOA between the overset and the FMG method : a) for $\alpha_0 = 5^\circ$ b) for different α_0 at $M = 0.15$ and $Re = 1.09 \cdot 10^6$ for the SACCON geometry

of sub-iterations was studied. A good convergence of the results is obtained for a time step of $\Delta t = 5 \cdot 10^{-6} s$ for the Gear method with 20 sub-iterations. In the case of the overset method, the Cartesian background mesh extends in all 3 directions over 40 chord lengths. The body-fitted mesh is positioned in the centre of this background mesh and extends over approximately 4 chord lengths (as shown in the Fig. 4). A domain of 20 chords length was used for the FMG method to perfectly capture the transient regime of the 3D SACCON geometry. The observed responses of the

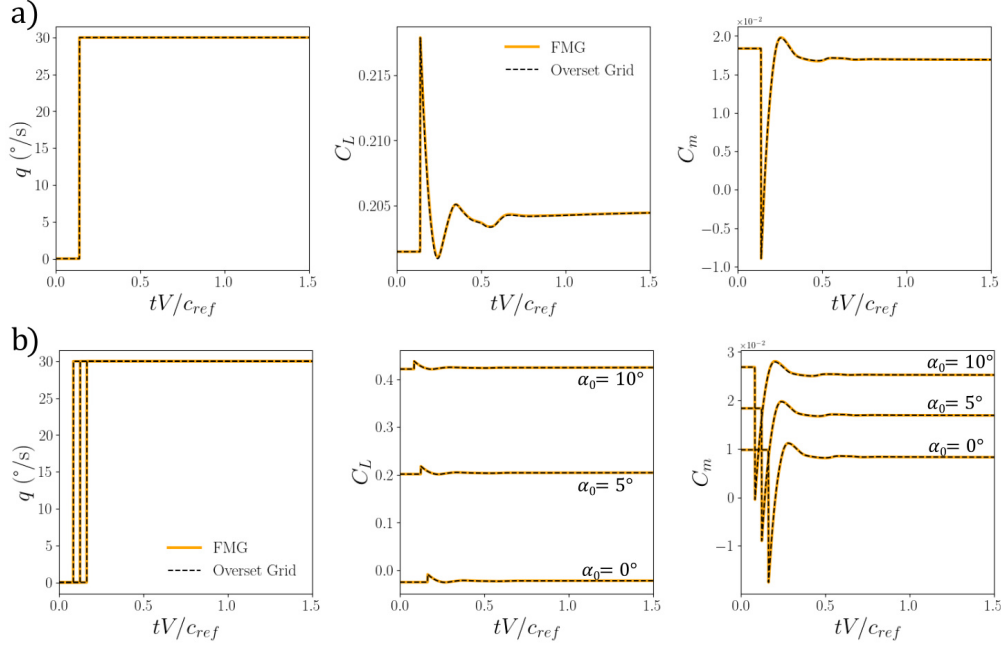


Fig. 9 Comparison of the time evolution of the lift and pitch coefficients due to a unit step change in the pitch rate between the overset and the FMG method : a) for $\alpha_0 = 5^\circ$ b) for different α_0 at $M = 0.15$ and $R_e = 1.09 \cdot 10^6$ for the SACCON geometry

system for an initial AOA of 5° for a unit step change in the AOA (Fig. 8a) or pitch rate step (Fig. 9a) show a near perfect superposition of the coefficients for FMG and overset methods. This comparison process was also carried out for different initial AOAs (Fig. 8b and 9b) and for each of them, the height of the peak, the duration of the transient regime and final asymptotic value are the same between both methods for the lift and the pitch coefficients. The indicial responses were then compared with the literature and in particular with the simulations performed on the SACCON geometry by Ghoreyshi et al. [23, 28]. The simulations are performed at $M = 0.15$ and $M = 0.3$. The results obtained with the FMG method are in agreement with Ghoreyshi et al. [23, 28]. Indeed, the height of the initial peak, the time of the transient regime as well as the asymptotic value reached in the stationary regime are almost identical (Fig. 10 a and b). For a positive unit step in AOA, when the grid starts to move, a positive peak in lift is observed whereas the peak is negative in the case of the pitching moment. The trend in the evolution of these coefficients can be explained by the disturbance of the flow around the SACCON caused by the sudden motion. This displacement leads to the rapid formation of compression and expansion acoustic waves on the lower and upper surfaces of the vehicle respectively, causing the overshoot on the coefficients [43]. As the simulation progresses and the motion becomes established, the waves move away from the vehicle and the coefficients asymptotically tend towards a steady-state value after about one convective time. In the case of an increasing Mach number, the initial peak of the response generally decreases with increasing compressibility effects. The results obtained show that the FMG method and the overset method give the same results and that for all AOAs. Then, these results are consistent with the literature. Moreover, the comparison between the two methods also showed that the FMG method is much faster on unsteady computations for equivalent mesh (Table 2). The duration of the URANS computations is reduced by around 50% in average for 3D case which represents a gain in terms of computational cost that is more than significant for equivalent results.

Mesh type	Number of cells	RANS CPU mean time (50000 iterations)	URANS CPU mean time (1000 iterations)
Overset grid	24 468 152	16h	8h30-9h
FMG	25 542 216	15h	4h30

Table 2 Comparison between numerical methods around the SACCON geometry

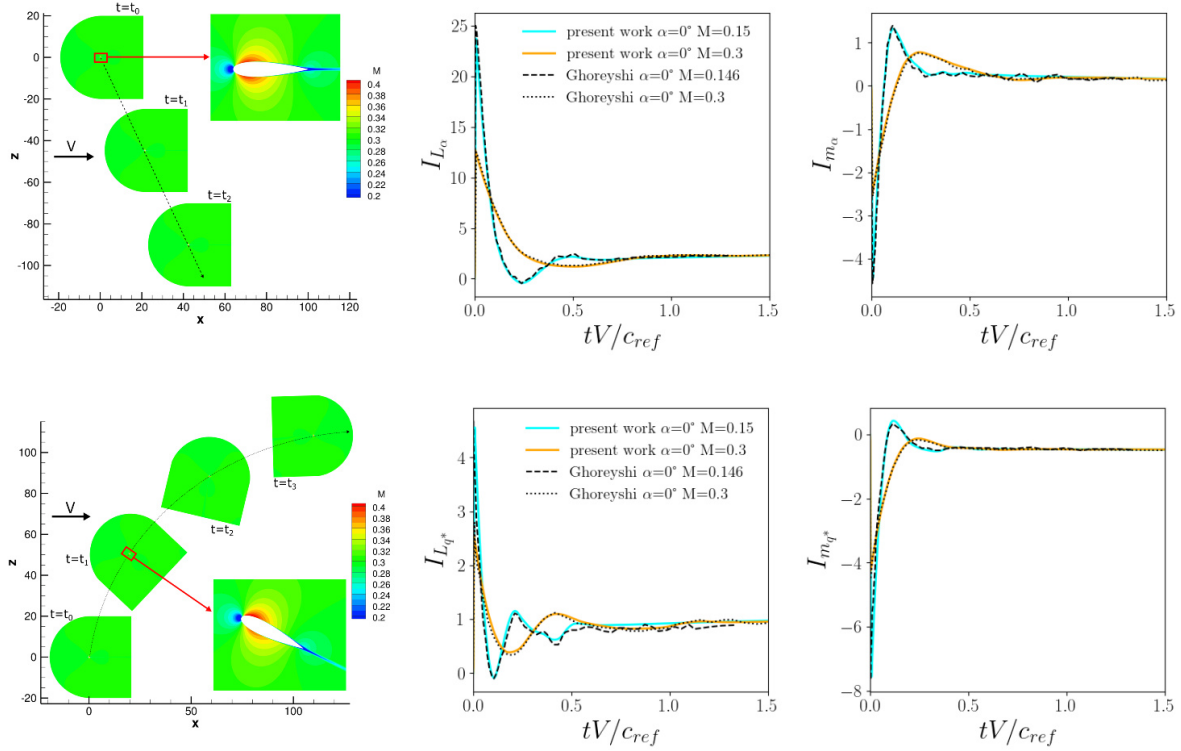


Fig. 10 Comparison between indicial responses of the SACCON geometry obtained in the present work at $M = 0.15$ and $R_e = 1.09 \cdot 10^6$ and those obtained by Ghoreyshi et al. at $M = 0.146$ and $M = 0.3$

C. Parameterised Indicial Responses

The indicial responses of the SACCON aircraft due to a positive step change in AOA and in the pitch rate are shown in figure 11. All calculations start with a steady-state solution at $M = 0.15$. For AOA responses, the motion starts at $t = 0s$ and the AOA increases by 1° . For pitch rate responses, the normalized pitch rate is increased by 0.5236 rad/s at $t = 0s$ and the AOA stays constant. It has been shown that indicial response has no significant sensitivity to the choice of the amplitude of the step of the AOA or the pitch rate [44]. The rotation center is chosen at the MRP. The linear indicial method (Eq. 3) can be applied without parameterised indicial responses. Indeed, the responses I_{i_α} and $I_{i_{q^*}}$ do not depend on the AOA. The linear model only needs the AOA and pitch rate responses at only one initial AOA chosen at 0° . In contrast, the non linear method depends on the initial AOA. To apply the non-linear model (Eq. 4), the present work shows simulations performed for 9 different AOAs ranging from -5° to 20° (Fig. 11) for both AOA responses and pitch rate responses. The figure 11) shows that indicial functions vary with the initial AOA. The initial values are invariant with initial AOA, but the transient trend and steady state values are different. The database is therefore made of AOA and pitch rate indicial responses which depend on the initial value of the AOA for positive step change. According to previous study [14], indicial responses for negative step change are also taken into consideration in the database to improve the model for both AOA and pitch rate. However, indicial responses need to be known for each initial AOA to apply the non linear model. That's why, the special approach of modelling based on time-dependent substitutes by Surrogate-based models presented by Ghoreyshi et al.[41] will be used. This method permits to interpolate the indicial

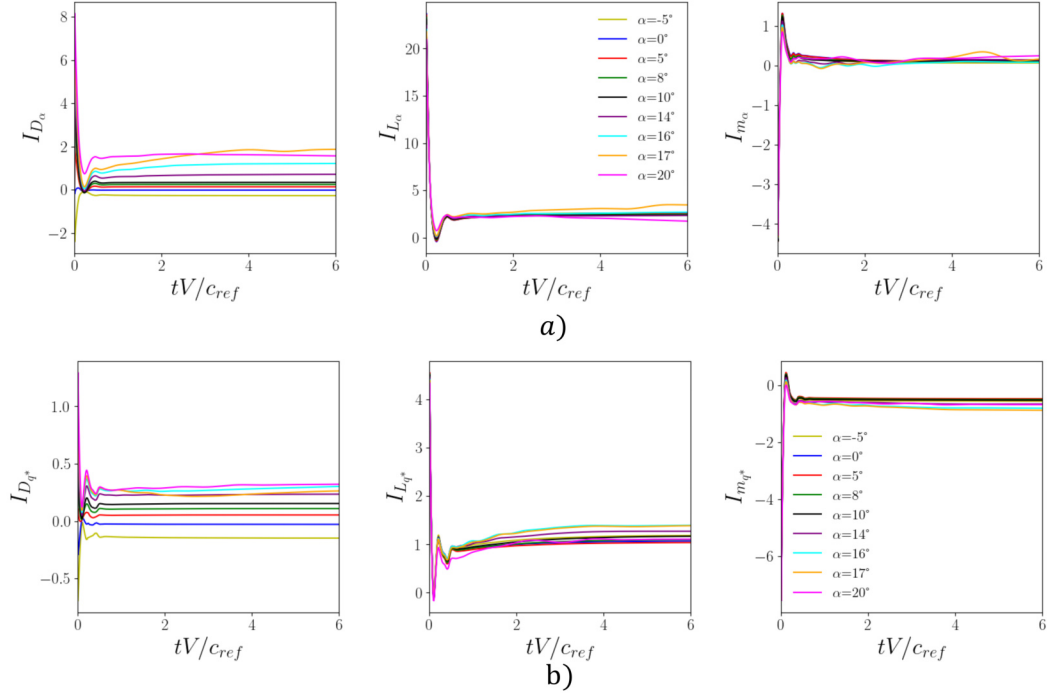


Fig. 11 Indicial simulation results for different initial AOAs: a) for a unit step change on the AOA, b) for a 30°/s step change on the pitch rate at $M = 0.15$ and $R_e = 1.09 \cdot 10^6$

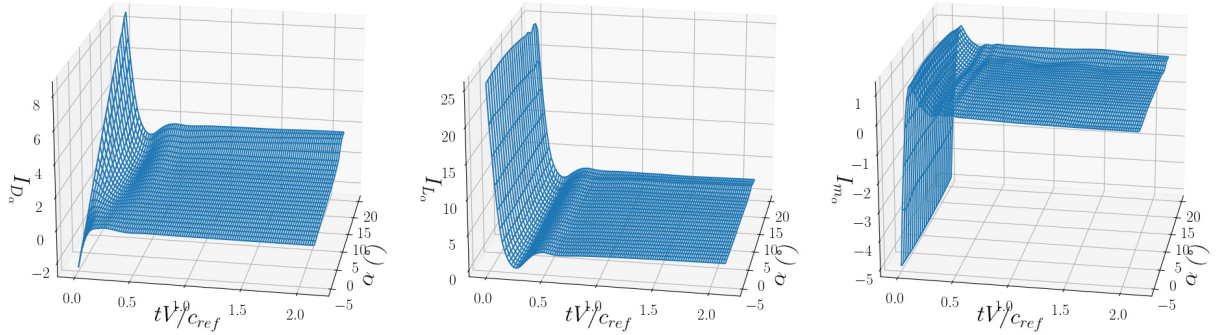


Fig. 12 Indicial responses obtained for each AOA between -5° and 20° from kriging interpolation for unit step change in AOA

response for AOAs that are not computed (Fig. 12). Similarly as in Ghoreyshi et al. [41], the indicial responses above 17° do not converge to a steady state probably due to the computational difficulties of our CFD simulations to catch the topology of the flow after the stall.

D. Forced oscillations

Forced pitch oscillation simulations were performed for different frequencies f (1Hz, 2Hz, 3Hz), for different mean angles α_m with an amplitude of $\alpha_k = 5^\circ$ (Fig. 13). The AOA at each time is given by $\alpha(t) = \alpha_m + \alpha_k \sin(2\pi ft)$. The aircraft is undergoing an oscillatory movement around a point distant from the nose of the aircraft of $0.438m$. The calculations are started with a steady-state solution at $M = 0.15$. During the forced oscillation, the aerodynamic coefficients are no longer equal to the static coefficients and are successively higher and lower or vice versa (Fig. 13). In the linear domain, the variations of the coefficients as a function of the AOA follow an ellipse whose axis is practically

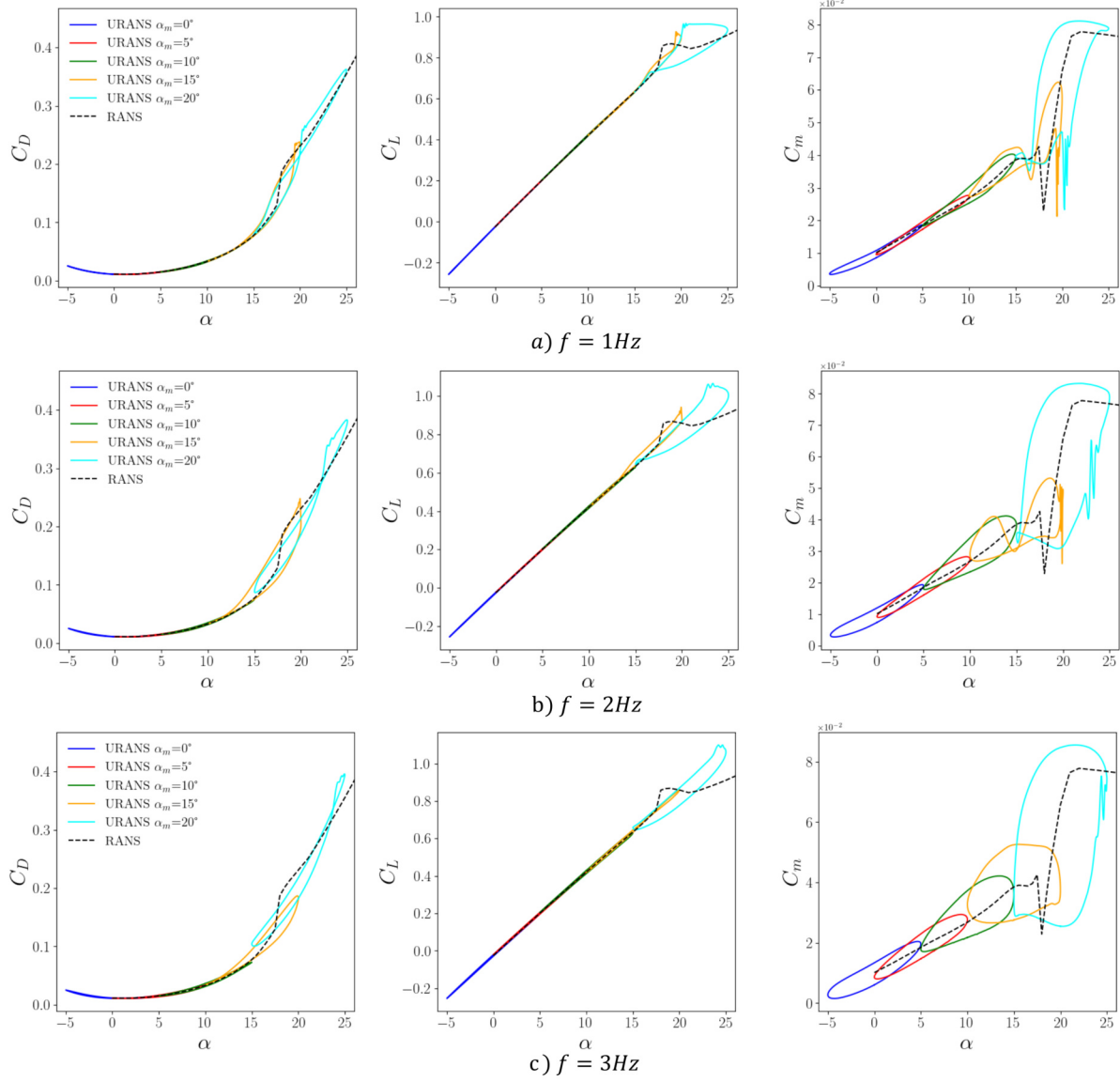


Fig. 13 Results of forced pitch oscillations of 5° amplitude centered in different AOAs α_m and for different frequencies at $M = 0.15$ and $Re = 1.09 \cdot 10^6$

aligned with the static curve. Hysteresis phenomena increases with the frequency which results in a thickening of the ellipses and a shift of its axis with respect to the static curve (Fig. 13). For forced oscillations with larger AOA (15-20°), the CFD predicts a strongly non-linear behaviour. The non-linearity is directly related to the vortex dynamics on the SACCON upper surface and in particular to the rise of the tip vortex and the position of the vortex breakdown. As the frequency increases, the non-linearities are smoothed and shifted to higher incidences. This is due to a lag on the evolution of the position of the vortices compared with the static case with the variation of the AOA. This phenomenon is very well observed in the case of the pitching moment drop which is almost not present at high frequency (C_m Fig. 13).

Simulations of pitch forced oscillations allow the identification of the different parameters of the linear quasi-steady and unsteady models. The coefficients of the quasi-static model are obtained by the method of the least squares performed separately on each oscillation and for each frequency. The obtained coefficients (Fig 14) show a dependence on the frequency at which the identification is performed. This dependence is most pronounced for high AOA but remains present for moderate AOA $\alpha < 10^\circ$. The quasi-static model therefore has the disadvantage of being evaluated and calibrated for a single frequency and so a rotation rate. The model will therefore be less accurate for a movement

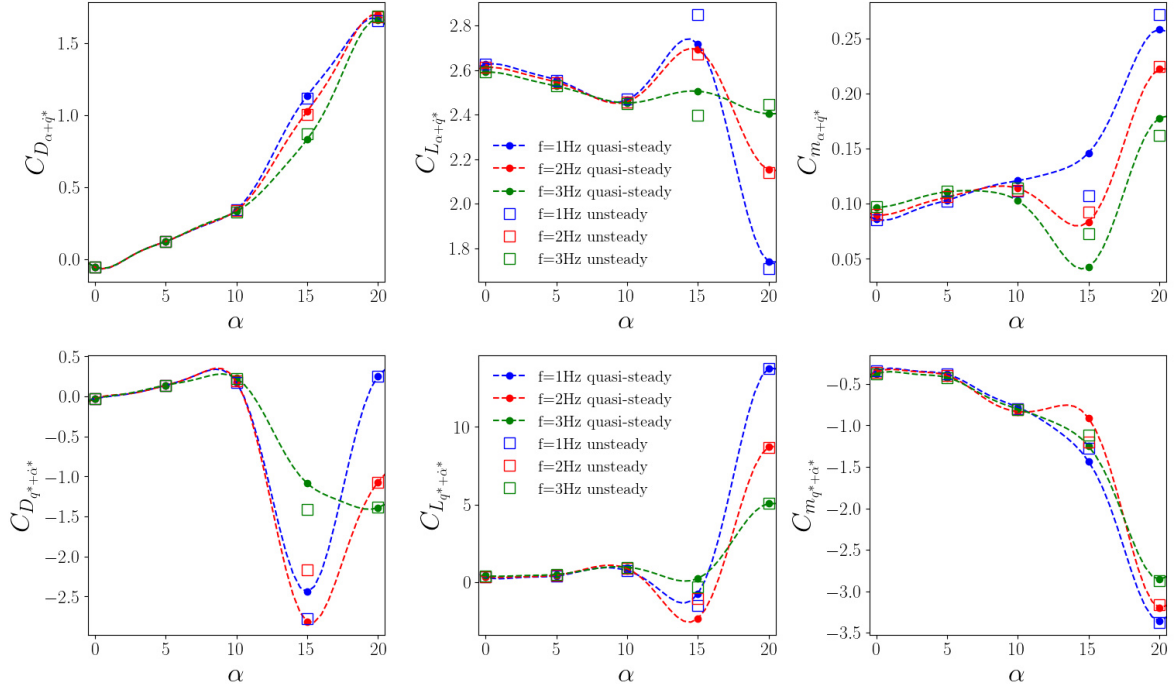


Fig. 14 Global static derivative and global damping coefficients as a function of the AOA and frequency

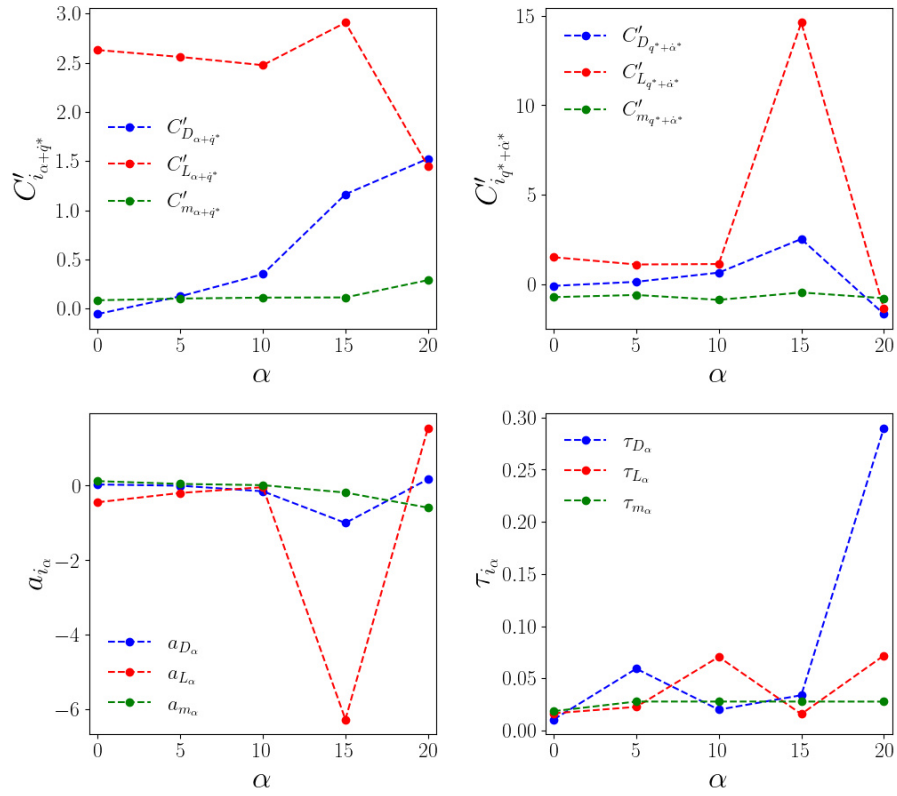


Fig. 15 Unsteady coefficients as a function of the AOA

with a different associated rotation rate.

This frequency dependence is taken into account in the unsteady linear model. The parameters of the model are identified by least squares on the forced oscillations for the 3 frequencies at the same time for a given mean AOA. The obtained coefficients are presented in figure 15. The unsteady coefficients are compared with the coefficients of the quasi-static model with Eq. (23) and plotted in figure 14. With the exception of the AOA of 15° , the unsteady model is able to reproduce the dependence on the frequency of the global static derivative $C_{i_{\alpha+q^*}}$ and global damping coefficient $C_{i_{q^*+\dot{\alpha}^*}}$ of the quasi-stationary model. Only the oscillation centered at 15° poses an identification problem (Fig. 14). For this incidence, the strongly non-linear character of the oscillation leads to a non-linearity in the frequency evolution of the coefficient. It is this non-linearity that the unsteady model fails to reproduce correctly. The linear unsteady model is therefore a good improvement to get away from this frequency dependence. It could be more profitable for the modelisation of any type of trajectory with different rotation rates. For the application of the linear quasi-stationary and unsteady models, the coefficients are interpolated by kriging method (Fig. 14).

E. ROM Applications

The accuracy of the previously implemented ROMs is evaluated in this section. The coefficients obtained from the ROMs during a forced oscillation are directly compared with the CFD calculation for different AOAs and frequencies. A percentage error of the ROMs will be calculated from the following formulation [14]:

$$C_i \text{ ROM error} = \frac{C_i^{ROM} - C_i^{CFD}}{|\max(C_i^{CFD}) - \min(C_i^{CFD})|} \times 100 \quad (24)$$

In this work, the linear quasi-steady model used is generated with 1Hz pitch oscillations (Fig. 13a) while the unsteady model is based on the three different frequencies simulated. A strong difference (until 30% for C_D , 4% for C_L and 30% for C_m) between ROM and CFD calculation is observed for AOAs below 0° (Fig. 17 a). This is caused by the extrapolation of the coefficients in this area. The longitudinal coefficients (C_D , C_L and C_m) obtained for both ROMs are very similar for 1Hz at low AOAs (Fig. 17 a and b). The accuracy of the quasi-steady model is slightly better at 1Hz compared with the unsteady model (Fig. 18 a and b). This is an expected result because the quasi-steady model is identified for this frequency. For a different frequency, the unsteady model is closer to CFD calculations (Fig. 17 a, b and c) and error compute is lower compared with the quasi-steady model (Fig. 18 a, b and c) especially for oscillation around 10° . The accuracy of the unsteady model compared with the quasi-steady model increases with the frequency and the increase of the AOA (Fig. 18 c). This is due to the increase of the frequency dependence with AOA while the quasi-steady model is build from a single frequency. The modelisation of the longitudinal coefficients by the linear unsteady ROM is quite good for positive AOAs up to 15° (error less than 10% for C_D , less than 6% for C_L and less than 10% for C_m). For higher AOAs, both linear ROMs are not able to reproduce the non-linearities present in the CFD calculations (Fig. 17c and 18 c). The calculated errors (Fig. 18) of the quasi-steady and unsteady models show that they perform well in modelling the C_D and C_L with deviations around 1% up to 10° . However, these ROMs fail to model the pitch coefficients C_m with errors mostly above 10%. The analysis of the evolution of the error also shows that the error increases with the frequency for the three coefficients. Besides, the shape and trends of the oscillations are not fully reproduced. Indeed, the error has a lemniscate-like shape (eight shaped curve Fig. 18). This shape means the ROMs predictions moves towards and away from the CFD solution without reproducing correctly the trends.

The linear indicial method requires very little simulation to be applied, but only performs well for AOAs close to 0° . As the AOA increases, the linear indicial method loses performance. Indeed, figure 16 shows a 1Hz pitch-oscillation case, with a mean AOA of 5° and an amplitude of 5° . The figure shows the nonlinear ROM predictions are in good agreement with CFD simulations, while linear ROM cannot predict correctly the evolution of the longitudinal coefficients. The errors on the longitudinal coefficients (Fig. 16b) show that the accuracy of the non-linear model is better compared with the linear indicial method. In addition, the figure 16a also shows that the indicial method is relatively accurate in predicting the transient regime of the SACCON aerodynamic coefficients at the beginning of the oscillation motion.

The non-linear method allows, in a range up to the wing stall (around 16°), to obtain very satisfactory results for the coefficients C_L and C_m (Fig. 19). Indeed, unlike the linear quasi-stationary and unsteady models (Fig. 17), the indicial method respects the evolution of CFD curves (Fig. 19). The calculated errors form ellipses, reflecting a kind of similarity between the shapes of ROM predictions and CFD calculations. Thus, for moderate AOAs up to 15° , the non-linear indicial method is able to reproduce correctly the trend of the coefficients C_L and C_m but shows some discrepancies in the values compared with CFD simulations. Indeed, an error of less than 8% for the C_L and less than 10% on the C_m is observed for AOAs up to 15° and for all frequencies (Fig. 20 a, b and c). Errors of 30% are observed

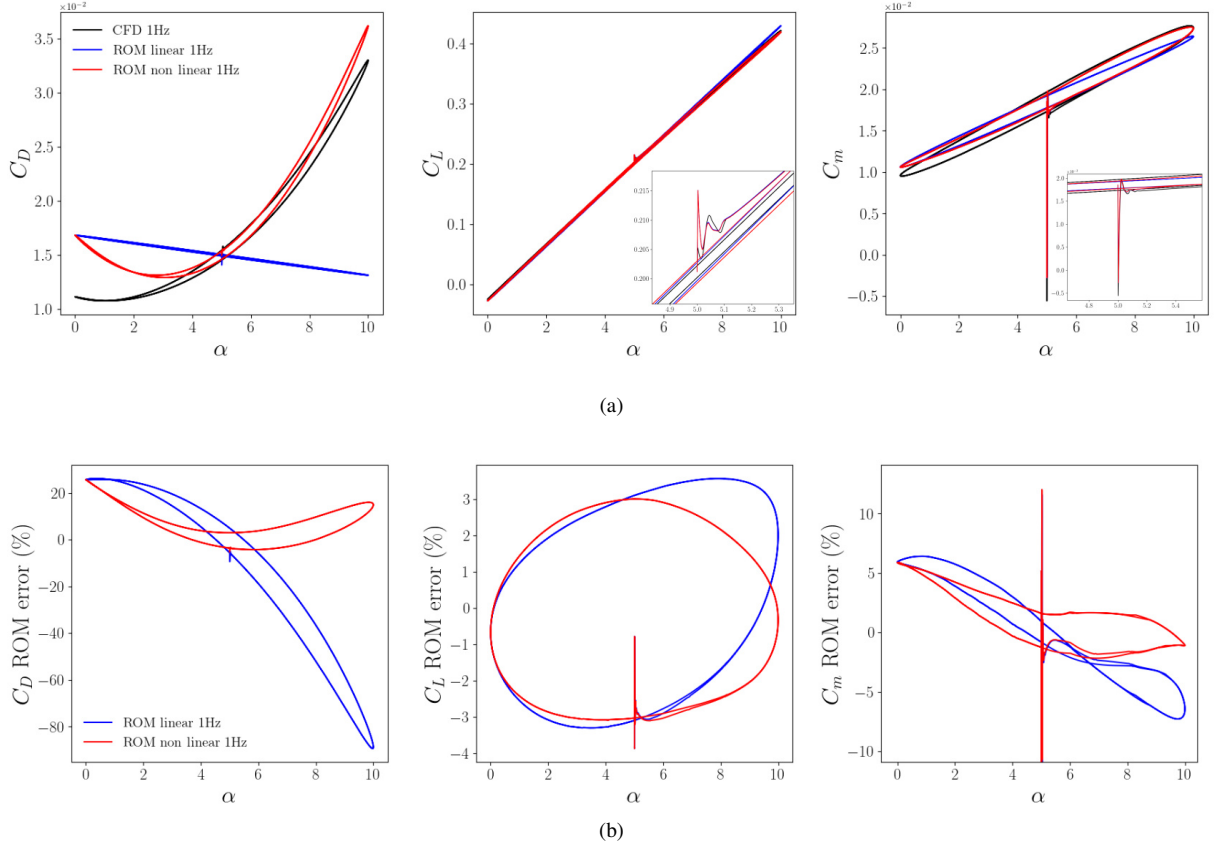


Fig. 16 Comparison between linear and nonlinear indicial methods for a 1 Hz pitch oscillation centered in $\alpha_m = 5^\circ$ for 5° amplitude of a) ROM coefficients b) error between ROMs and CFD simulations

on the C_D . Above 15° , the indicial responses no longer converge to a steady state, leading to major differences in the coefficients at high incidence. This could be induced by the wing stall, the rise and/or the breakdown of the tip vortex. Contrary to linear quasi-steady model and unsteady model, the increase of the frequency does not necessarily lead to an increase in the measured error. Indeed, the error decreases for the lift coefficient (Fig. 20).

The comparison between the CFD ROMs shows that the non-linear indicial method is the most suitable to reproduce a correct behaviour of the UCAV. The errors measured on the C_L and C_D coefficients are higher than those of the quasi-steady and unsteady model. However, the indicial method generates a better modelisation of the pitch coefficient and a better reproduction of the trends in the evolution of the three longitudinal coefficients for all frequencies. The implementation cost of the non linear method is expensive, higher than the implementation of the quasi-steady model but lower than the unsteady model (Table 3). Thus, for a low incidence simulation, the inexpensive linear indicial model seems sufficient. In the case of simulation in the linear domain with rotation rates that do not vary much, the quasi-stationary linear model seems appropriate for a low cost model. Otherwise the non-linear model will be better recommended to model correctly the behaviour of the aircraft. For a trajectory simulation, the unsteady model or the non-linear model can be chosen because both models are independent of the frequency and so of the rotation rate. However, the unsteady model is more expensive and gives less accurate results in the evolution of the coefficients and on the prediction of the pitch coefficient compared with the non-linear indicial method. The indicial method seems to be the most appropriate ROM to model correctly the longitudinal coefficients, despite the small discrepancies in the obtained values. Once the longitudinal ROMs are constructed, a rapid prediction of a wide range of pitching and plunging motions can be performed. The computational cost of only one CFD simulation is less than the implementation cost of each ROMs. So, the more trajectory simulations are performed, the more cost-effective the ROM will be.

ROM	Simulation types	Number of AOA	Total Training time/CPU (h)	Executing time (min)
Linear indicial	α, q positive step	1	72	1
Non-linear indicial	α, q positive and negative step	9	1296	15
Linear quasi-steady 1Hz	1 frequency (2 cycles)	5	300	1
Linear quasi-steady 2Hz	1 frequency (2 cycles)	5	450	1
Linear quasi-steady 3Hz	1 frequency (2 cycles)	5	900	1
Linear unsteady	3 frequencies (2 cycles)	5	1650	1

Table 3 Computational cost comparisons

VI. Conclusion and prospects

This paper presents several approaches to model the unsteady and non-linear longitudinal aerodynamics of a UCAV configuration thanks to CFD simulations using grid motions. In order to minimize the cost of implementation the reduced order models studied, a new and less expensive method of grid movement was applied. This new method compared with the overset approach is twice as fast, for equivalent results. The method has been applied to the SACCON geometry and compared with the literature.

Indicial and forced oscillation simulations were performed to establish a database of the various ROM parameters. A comparison between the linear quasi-steady model, the unsteady model, the indicial method and the CFD simulations has been carried out.

The results show that the linear quasi-steady model generated from 1Hz forced oscillations and the unsteady model generated from three different frequencies of oscillations reproduce well the lift and drag coefficient. More difficulties are encountered to model the pitching moment. With the increase of the frequency and the AOA, the unsteady model becomes more efficient than the quasi-steady model. In addition, the evolution of the trends of the coefficients are not well respected.

The non-linear indicial method most accurately reproduces the trends and shape of the evolution of the longitudinal coefficients despite deviations that may be slightly larger than the linear quasi-stationary and unsteady ROMs. The results show a good agreement, with small discrepancies, of the non-linear indicial method with the CFD calculation until the wing stall around 16° . Furthermore, it has been shown that the implementation cost of the indicial method is not too expensive compared with the other ROM studied.

Future work will aim to improve the models studied. For the linear quasi-steady and unsteady models, the main goal will be to decouple the coefficients. For this purpose, specific CFD computations will be performed by imposing a periodic oscillation motion on only one parameter. In a similar way to the indicial simulations, imposing the following conditions allow to study the influence of $\dot{\alpha}$ only, without the influence of the pitch rate q :

$$\alpha(t) = \begin{cases} \alpha = \alpha_0 + \alpha_k \sin(2\pi f t) & \text{if } t > 0 \\ \alpha = \alpha_0 & \text{else} \end{cases} \quad p, q, r = 0 \text{ rad/s}, V = \text{cst}$$

For the indicial method, the aim will be to understand the origins of the discrepancies observed. In this work, the centers of rotation of forced oscillations and indicial simulations are different. Thus, a study on the influence on the indicial responses of the center of rotation will be achieved. As it stands, the indicial method only takes into account the effects of the AOA and the pitching caught alone. The influence of $C_{i\alpha^*}$ is not taken into account. Thus, the influence of this coefficient on the accuracy of the model will be studied.

Then these ROMs will be extended to the modelling of lateral aerodynamics and finally applied and compared on some realistic 6-DOF aircraft manoeuvres.

VII. Acknowledgment

The authors gratefully acknowledge the financial support given by ONERA and the region Hauts-de-France. The authors appreciate the support provided by the elsA software technical assistance and the help of Julien Dandois for the application of the overset method. SACCON (Stability and Control Configuration) geometry and wind-tunnel data were provided by NATO RTO Task Group AVT-161 on Assessment of Stability and Control Prediction Methods for NATO Air and Sea Vehicles.

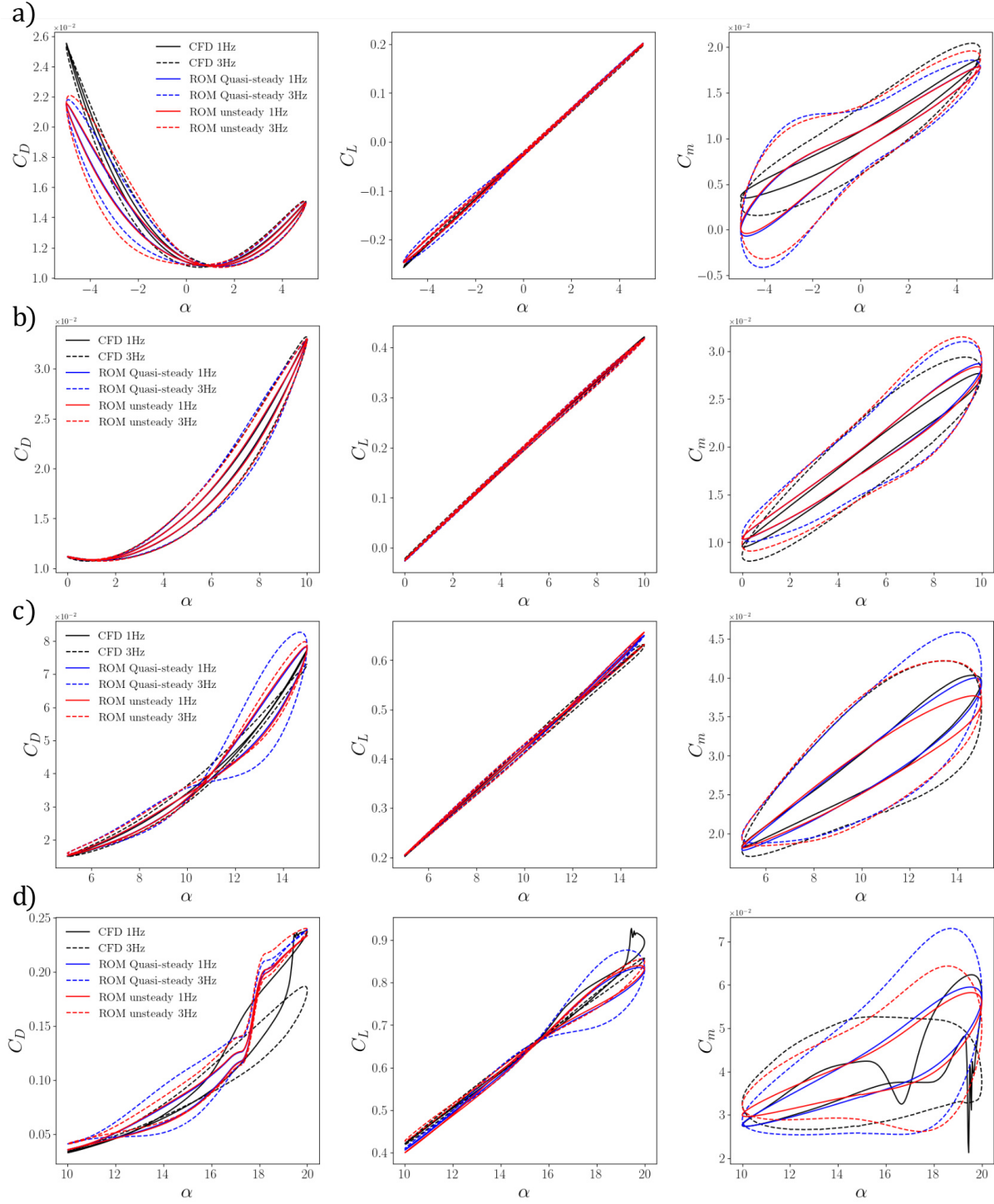


Fig. 17 Comparison between linear quasi-steady, unsteady model predictions with CFD simulations for 1Hz and 3Hz forced oscillations of 5° amplitude centered in a) 0°, b) 5°, c) 10° and d) 15°

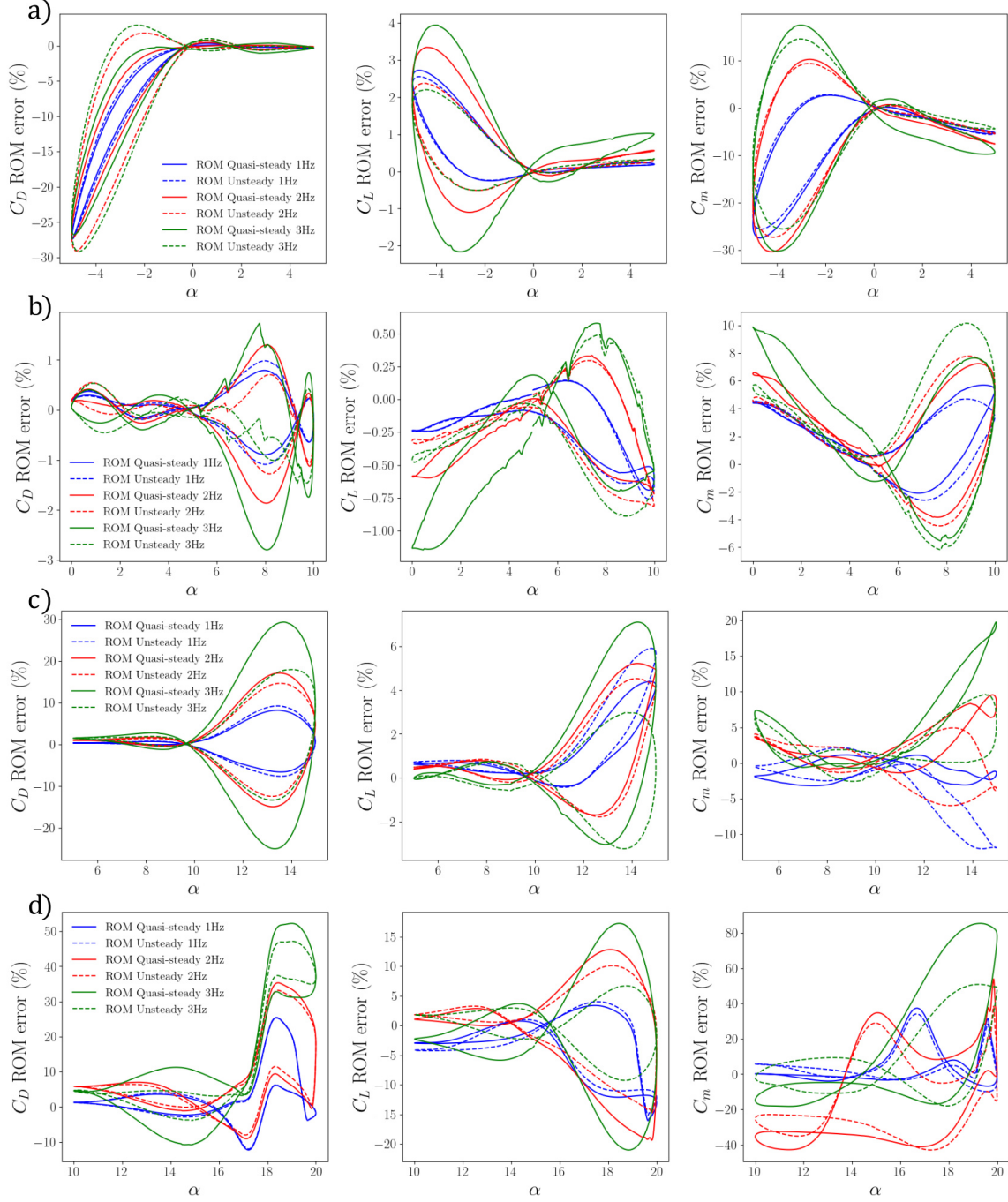


Fig. 18 Errors between the predictions of the linear quasi-steady, unsteady models with the CFD simulations for 1Hz, 2Hz and 3Hz forced oscillations of 5° amplitude centered in a) 0°, b) 5°, c) 10° and d) 15°

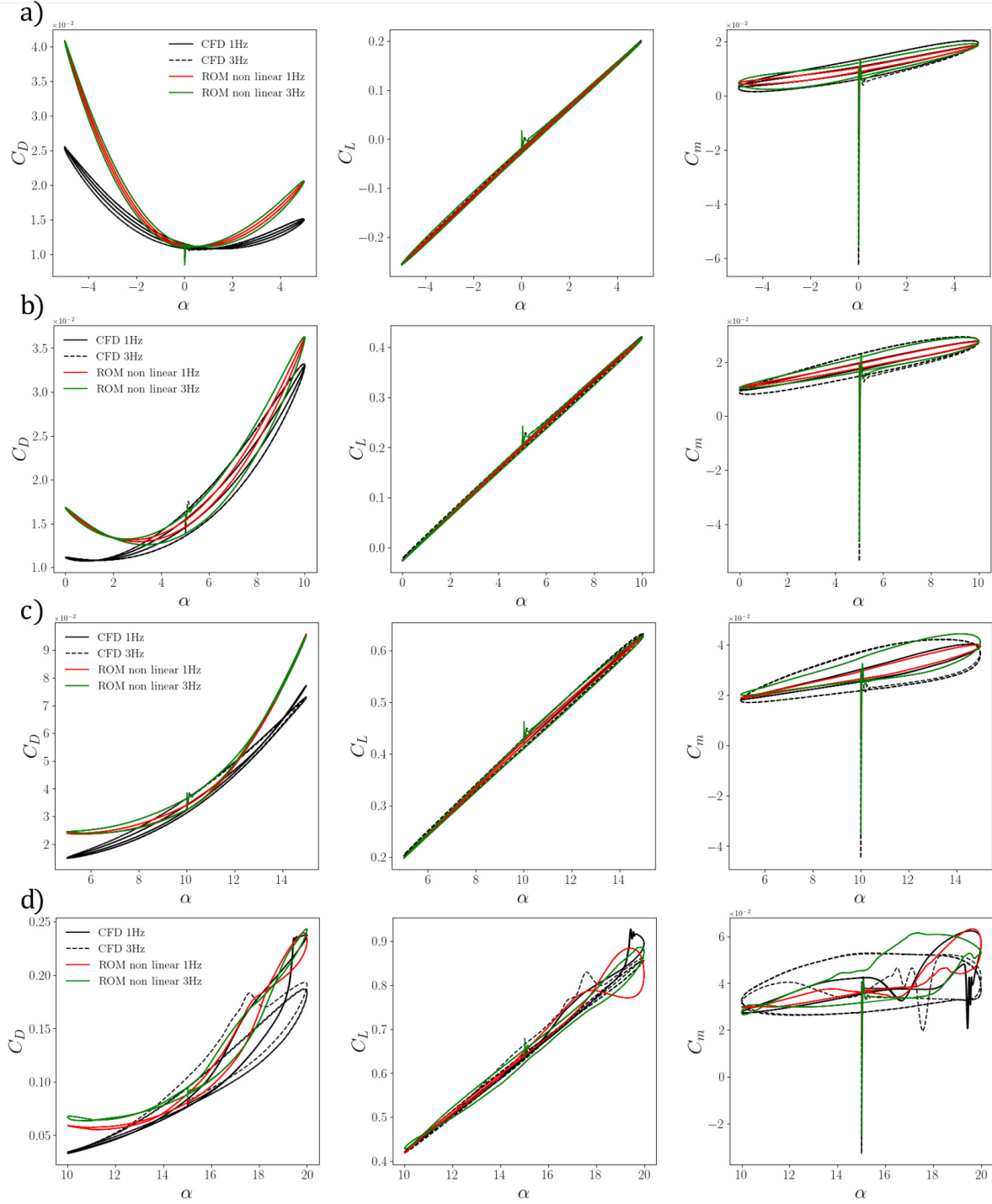


Fig. 19 Comparison between non-linear indicial method predictions and CFD simulations for 1Hz and 3Hz forced oscillations of 5° amplitude centered in a) 0°, b) 5°, c) 10° and d) 15°

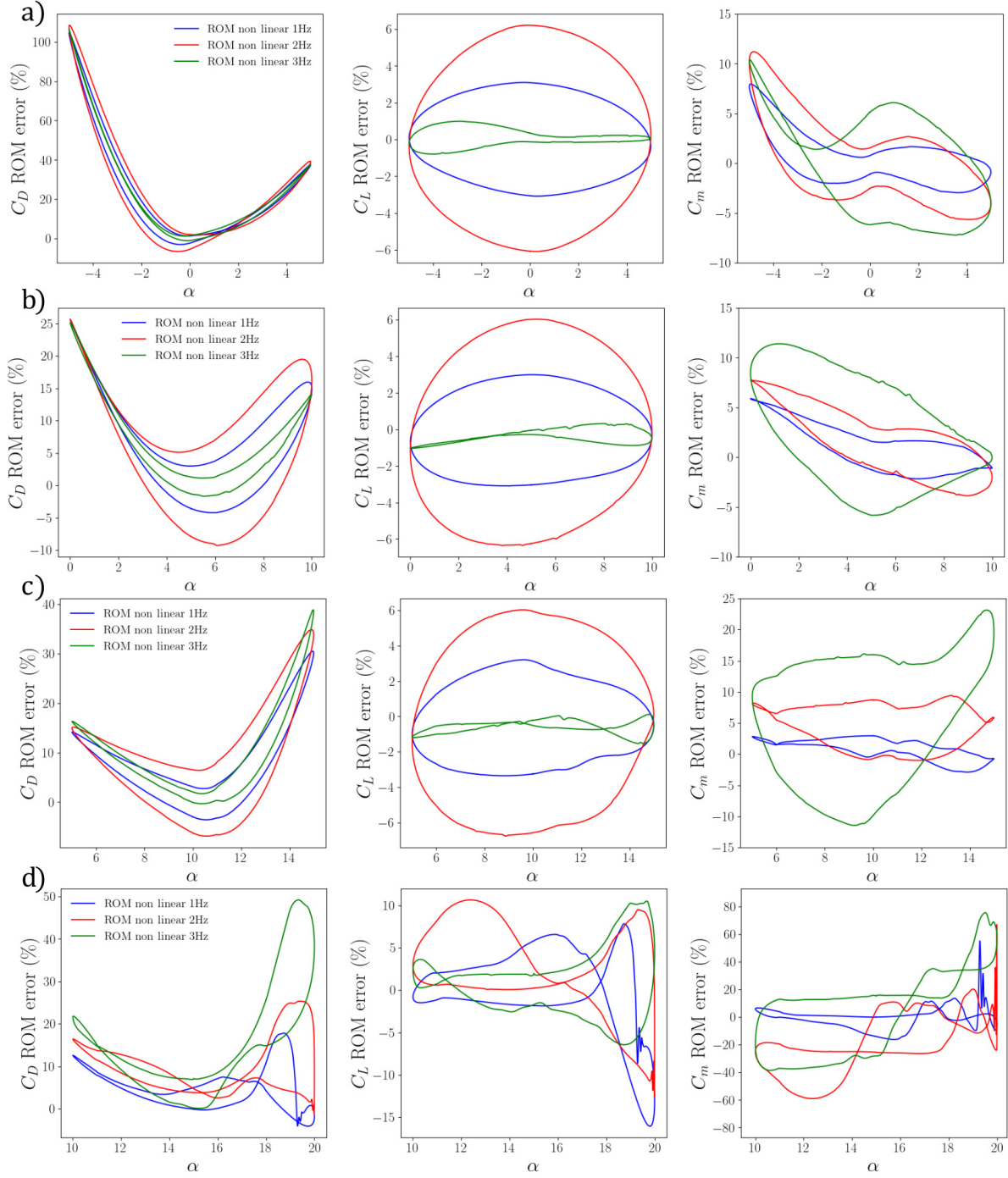


Fig. 20 Errors between the predictions of the non-linear indicial model and the CFD simulations for 1Hz, 2Hz and 3Hz forced oscillations of 5° amplitude centered in a) 0°, b) 5°, c) 10° and d) 15°

References

- [1] Foster, J., Cunningham, K., Fremaux, C., Shah, G., and al., E. S. ., “Dynamics Modeling and Simulation of Large Transport Airplanes in Upset Conditions,” *AIAA Paper 2005-5933*, 2005.
- [2] Myatt, J. H., Schumacher, C. J., and P. D. McKeehen, J. B., “Modeling and simulation of unsteady aerodynamic effects on a tailless aircraft,” *AIAA paper 98-4455*, 1998.
- [3] Abramov, N., Goman, M., Greenwell, D., and Khrabrov, A., “Two Step Regression Method for Identification of High-Incidence Unsteady Aerodynamic Model,” *AIAA Atmospheric Flight Mechanics Conference and Exhibit*, AIAA, 2001.
- [4] Planckaert, L., “Model of Unsteady Aerodynamic Coefficients of a Delta Wing aircraft at high angles of attack,” *Symposium RTO «Advanced Flow Management »*, 2001.
- [5] Ghoreyshi, M., and Cummings, R. M., “Unsteady Aerodynamics Modeling for Aircraft Maneuvers: a New Approach Using Time-Dependent Surrogate Modeling,” *30th AIAA Applied Aerodynamics Conference*, 2012.
- [6] Irving, J., “Development of an Aerodynamic Simulation Model of a Generic Configuration for S&C Analyses,” *AIAA paper*, 2014.
- [7] Morgand, S., “Caractérisation et contrôle de l’écoulement autour d’un UCAV générique..” *Thesis, Université Pierre et Marie Curie - Paris VI*, 2013.
- [8] Vallespin, D., “Development of a process and Toolset to Study UCAV Flight Mechanics using Computational Fluid Dynamics,” *PhD Thesis, University of Liverpool, UK*, 2011.
- [9] Roy, J.-F. L., Morgand, S., and Farcy, D., “Static and Dynamic Derivatives on Generic UCAV without and with Leading Edge Control,” *32nd AIAA Applied Aerodynamics Conference*, 2014.
- [10] Rohlf, D., Schmidt, S., and Irving, J., “Stability and Control Analysis for an Unmanned Aircraft Configuration Using System-Identification Techniques,” *Journal of Aircraft*, 2012.
- [11] Cummings, R., and Schutte, A., “Detached-Eddy Simulation of the Vortical Flowfield about the VFE-2 DeltaWing,” *46th AIAA Aerospace Sciences Meeting and Exhibit, (AIAA Paper 2008-396)*, 2008.
- [12] Cummings, R. M., Schutte, A., and Hubner, A., “Overview of Stability and Control Estimation Methods from NATO STO Task Group AVT-201,” *51st AIAA Aerospace Sciences Meeting*, 2013.
- [13] Greenwell, D. I., “A review of unsteady aerodynamic modelling for flight dynamics of manoeuvrable aircraft,” *AIAA paper 2004-5276*, 2004.
- [14] Hiller, B., *An Unsteady Aerodynamics Reduced-Order Modeling Method For Maneuvring, Flexible Flight Vehicles*, PhD thesis, Thèse de doctorat de Georgia Institute of Technology, USA, 2019.
- [15] Allen, J. D., Ghoreyshi, M., Jirásek, A., and Satchell, M. J., “Aerodynamic Loads Identification and Modeling of UCAV Configurations with Control Surfaces Using Prescribed CFD Maneuvers,” *2018 Applied Aerodynamics Conference*, 2018.
- [16] Bommanahal, M. V., *Nonlinear Modeling and Identification of Unsteady Aerodynamics at Stall*, PhD thesis, Thèse de doctorat Faculty of Technology, De Montfort University, UK, 2015.
- [17] Kirschstein, S., and Alles, W., “Identification of Dynamic Derivatives with a Controlled Wind Tunnel Model of the Spaceplane-Configuration PHOENIX,” *Aerospace Science and Technology*, 2004.
- [18] Kyle, H., Lowenberg, M., and Greenwell, D. I., “Comparative evaluation of unsteady aerodynamic modeling approaches,” *AIAA paper 2004-5272*, 2004.
- [19] Goman, M. G., and Khrabrov, A. N., “State-space representation of Aerodynamic Characteristics of an Aircraft at High-angle-of-attack,” *AIAA Journal of Aircraft*, Vol. 31, No. 5, pp. 1109–1115., 1994.
- [20] Abramov, N. B., Goman, M. G., Khrabrov, A. N., and Kolinko, K. A., “Simple Wings Unsteady Aerodynamics at High Angle of Attack: Experimental and Modeling Results,” *AIAA Atmospheric Flight Mechanics Conference and Exhibit*, AIAA, 1999.
- [21] Klein, V., and Noderer, K. D., “Modeling of Aircraft Unsteady Aerodynamic Characteristics, part1,” *NASA. Langley Research Center*, 1994.

- [22] Ghoreyshi, M., Jirasek, A., Post, M. L., Cummings, R. M., and Decker, R. K., "A Computational Investigation into the Use of Response Functions For Aerodynamic Loads Modeling," *29th AIAA Applied Aerodynamics Conference*, 2011.
- [23] Ghoreyshi, M., Jirásek, A., and Cummings, R. M., "Reduced order unsteady aerodynamic modeling for stability and control analysis using computational fluid dynamics," *Progress in Aerospace Sciences* 71 167-217, 2014.
- [24] Tobak, M., Chapman, G., and Schiff, L., "Mathematical modeling of the aerodynamic characteristics in flight dynamics," *NASA TN-85880*, 1984.
- [25] Tobak, M., and Chapman, G., "Nonlinear problems in flight dynamics involving aerodynamic bifurcations," *NASA TN-86706*, 1985.
- [26] Reisenthel, P., "Development of a nonlinear indicial model using response functions generated by a neural network," *AIAA paper 97-0337*, 1997.
- [27] Reisenthel, P., "Data-based aerodynamic modeling using nonlinear indicial theory," *AIAA paper 97-0337*, 1999.
- [28] Ghoreyshi, M., Young, M. E., Jirasek, A., Lofthouse, A. J., and Cummings, R. M., "Validation of Unsteady Aerodynamic Models of a Generic UCAV Using Overset Grids," *AIAA 2014-2265. 32nd AIAA Applied Aerodynamics Conference*, June 2014.
- [29] Ronch, A. D., Ghoreyshi, M., and al., R. C. ., "Modeling of unsteady aerodynamic loads," *AIAA Atmospheric Flight Mechanics Conference*, p. 6524, 2011.
- [30] Cambier, L., and Veillot, J.-P., "Status of elsa software for flow simulation and multidisciplinary applications," *46th AIAA Aerospace Science Meeting and Exhibit*, 2008.
- [31] Cambier, L., Heib, S., and Plot, S., "The onera elsa cfd software : input from research and feedback from industry," *volume eFirst*, 2013.
- [32] Roache, P. J., "Perspective: A Method for Uniform Reporting of Grid Refinement Studies," *Journal of Fluids Engineering*, 116, 405-413, 1994.
- [33] Spalart, P., and Allmaras, S., "A one-equation turbulence model for aerodynamic flows," *Recherche Aerospaciale, No. 1*, pp. 5-21, 1994.
- [34] Jameson, A., Schmidt, W., and Turkel, E., "Numerical solution of the Euler equations by finite volume methods using Runge Kutta time stepping schemes," *14th Fluid and Plasma Dynamics Conference*, 1981.
- [35] Choi, Y., and Merkle, C., "The Application of Preconditioning in Viscous Flows," *Journal of Computational Physics*, 105: 207-223, 1993.
- [36] Weiss, J., and Smith, W., "Preconditioning applied to variable and constant density flows," *American Institute of Aeronautics and Astronautics Journal*, 33(11) :2050-2057, 1995.
- [37] Ahmad, J., and Duque, E. P., "Helicopter Rotor Blade Computation in Unsteady Flows Using Moving Overset Grids," *Journal of Aircraft, Vol. 33, No. 1*, 1996.
- [38] Ghoreyshi, M., and Cummings, R. M., "Aerodynamics modeling of a maneuvering aircraft using indicial functions," *50th AIAA Aerospace Sciences Meeting*, pp. 1012-689, 2012.
- [39] Pang, C., Gao, Z., Yang, H., and Chen, S., "An efficient grid assembling method in unsteady dynamic motion simulation using overset grid," *Aerospace Science and Technology*, 2021.
- [40] Ghoreyshi, M., Jirasek, A., and Cummings, R. M., "Computational investigation into the use of response functions for aerodynamic-load modeling," *AIAA journal*, vol. 50, no. 6, pp. 1314-1327, 2012.
- [41] Ghoreyshi, M., Jirasek, A., and Cummings, R. M., "Reduced order unsteady aerodynamic modeling for stability and control analysis using computational fluid dynamics," *Progress in Aerospace Sciences*, vol. 71, pp. 167-217, 2014.
- [42] Gray, J. S., Hwang, J. T., Martins, J. R. R. A., Moore, K. T., and Naylor, B. A., "OpenMDAO: An open-source framework for multidisciplinary design, analysis, and optimization," *Structural and Multidisciplinary Optimization*, Vol. 59, No. 4, 2019, pp. 1075-1104. <https://doi.org/10.1007/s00158-019-02211-z>.
- [43] Mangano-Villamarin, C. E., and Shaw, S. T., "Three-Dimensional Indicial Response of Finite Aspect Ratio Yawed Wings," *The Aeronautical Journal*, Vol. 111, No. 1120, pp. 359-371, 2007.
- [44] Raveh, D., "Reduced-order models for nonlinear unsteady aerodynamics," *AIAA journal*, vol. 39, no. 8, pp. 1417-1429, 2001.